MORC2 directs transcription-dependent CpG methylation of human LINE-1 transposons in early neurodevelopment

Fereshteh Dorazehi,[1] Caterina Francesconi,[1]# Ninoslav Pandiloski,[1,2]# Laura Castilla-Vallmanya,[2]# Anna Albecka,[3,4] Symela Koutounidou,[1] Sivani Bala Mohan,[1] Anita Adami,[2] Angelos Katsikas,[1] Jana Matijević,[1] Ofelia Karlsson,[2] Carrie Davis-Hansson,[2] Jenny G. Johansson,[2] Yorgo Modis,[3] Johan Jakobsson,[2] Christopher H. Douse[1]*

# these authors contributed equally

* correspondence: christopher.douse@med.lu.se

1. Lab of Epigenetics and Chromatin Dynamics, Lund Stem Cell Center and Section of Neurobiology, Department of Experimental Medical Science, Lund University, Sweden.
2. Lab of Molecular Neurogenetics, Lund Stem Cell Center and Section of Neurobiology, Department of Experimental Medical Science, Lund University, Sweden.
3. Molecular Immunity Unit, Department of Medicine, University of Cambridge, MRC Laboratory of Molecular Biology, Cambridge, U.K.
4. Present address: MRC Laboratory of Molecular Biology, Cambridge, U.K.

ABSTRACT.

Methylation of CpG dinucleotides is essential for silencing genomic repeats such as LINE-1 retrotransposons (L1s) in the germline and soma. Evolutionarily-young L1s are transcribed in human pluripotent stem cells, but how CpG methylation is patterned to these L1s upon exit of pluripotency is unknown. Here we investigate the critical functions of chromatin regulator MORC2 in epigenome reprogramming of the repetitive genome in early human neurodevelopment. We find that reversible ATP-dependent dimerization is required for MORC2 accumulation over L1s but not gene promoters. Mutation of the MORC2 ATPase module, causative for neurodevelopmental disorders, severely disrupts the distribution of MORC2 chromatin binding, leading to simultaneous loss of L1 transcriptional control and hyper-repression of clustered ZNF genes in human pluripotent stem cells. Upon neural differentiation these phenotypes persist due to striking, targeted defects in CpG methylation patterning. Together our results define the vital role of MORC2 in safeguarding the somatic human genome upon exit of pluripotency by directing CpG methylation patterning over transcriptionally-active retrotransposons in a manner analogous to the piRNA pathway in the germline.

33 **INTRODUCTION.**

34 Transposable elements (TEs) – in particular, retrotransposons such as long interspersed
35 nuclear element 1 (L1) – have accumulated in mammalian genomes and account for at least
36 half of human DNA.[1] Out of more than half a million fixed L1s in the reference genome, around
37 two thousand hominoid-specific copies retain an intact internal promoter and are thus
38 competent for transcription. These elements are a source of novel transcripts in human
39 tissues.[2–5] A smaller subset of around 100 human-specific L1s encode proteins that enable
40 transposition of their own and other TE transcripts to new sites, resulting in polymorphisms
41 within and between individuals.[6,7] Older L1 fragments lacking their own promoter often reside
42 in introns of transcribed genes where they can influence mRNA processing and gene
43 expression.[8–11] L1 activity is therefore responsible for substantial genetic and transcriptional
44 variation in the human population.

45 Unrestricted mobilization of L1s and other TEs is deleterious and transcription of intact
46 sequences is controlled by promoter CpG methylation in somatic mammalian cells.[12–15] As
47 part of the epigenetic reprogramming that happens during germ cell and embryonic
48 development, when TE transcription is transiently tolerated and in certain cases functionally
49 important,[16–20] DNA methylation patterns are reestablished after periods of global erasure. In
50 the germline, the piRNA pathway licenses transcription-dependent TE methylation.[21] In
51 embryonic stem cells, the most studied mechanism of restriction works via the KRAB zinc-
52 finger (KRAB-ZNF) family of transcription factors, which bind to specific TE DNA sequences
53 and recruit the TRIM28 corepressor that promotes histone 3 lysine 9 trimethylation
54 (H3K9me3) and CpG methylation.[22,23] KRAB-ZNF genes have rapidly diversified by segmental
55 duplication during vertebrate evolution to recognize TE and repeat family sequences.[24,25]
56 However, in the human setting, it is thought the youngest L1 subfamilies have evaded this
57 DNA-directed silencing system: changes in the ancestral L1PA3 promoter allowed subsequent,
58 evolutionarily-younger L1 copies to escape silencing by ZNF93.[26,27] In human pluripotent stem
59 cells, L1 expression is indeed mostly restricted to human-specific (L1HS) and hominoid-
60 specific (L1PA2/3) elements, which correlates with relative promoter hypomethylation and
61 varies between individual integrants.[28–30] Although lineage-specific L1-driven transcripts exist,
62 and intronic L1s are passively transcribed in pre-mRNA of thousands of genes, CpG
63 methylation mostly silences the promoters of the youngest, intact L1s in somatic human

64 tissues.[13,31] How methylation is patterned to young L1 promoters upon exit of pluripotency
65 and differentiation has been an open question but is not thought to depend solely on the
66 KRAB-ZNF/TRIM28 system.

67 A key player in the regulatory relationship (sometimes referred to as an 'arms race'[26])
68 between L1s and KRAB-ZNF genes is the chromatin remodelling ATPase MORC2.[8,32] In
69 collaboration with the human silencing hub (HUSH) complex, MORC2 is recruited to repress
70 transcriptionally-active L1s and repetitive gene clusters, including those encoding KRAB-ZNFs,
71 at H3K9me3-marked sites.[8,32–35] ChIP-seq experiments in cancer cell lines also identified a
72 second class of MORC2 peaks over transcription start sites, the functional significance of
73 which is unknown.[32] MORC2 contains an N-terminal ATPase module that reversibly dimerizes
74 upon ATP binding and hydrolysis, and a C-terminal coiled coil domain that forms constitutive
75 dimers.[36–38] Elegant recent experiments with purified components have shown that MORC2
76 binds and entraps free and nucleosomal DNA between these dimerization domains in a length
77 but not sequence-dependent manner, forming loops and multimeric assemblies that compact
78 the underlying chromatin.[36] This mechanism of MORC chromatin remodelling appears to be
79 conserved at least across the animal kingdom[39] and perhaps more deeply – MORCs are
80 encoded in plant, basal eukaryote and even prokaryote genomes.[40–43]

81 MORC2 functions are vital to human health: predicted loss of function alleles are strongly
82 selected against in the population[44] and heterozygous missense mutations in the MORC2
83 ATPase module cause severe neurodevelopmental disorders with symptoms including
84 intellectual disability and cerebellar ataxia.[45–47] Patient mutations cause changes to the
85 protein's enzymatic activity and hyperrepression of clustered KRAB-ZNF genes in cancer cell
86 lines.[32] A recent paper profiling peripheral blood and fibroblasts from patients with MORC2
87 mutations revealed an 'episignature' corresponding to hypermethylation and repression of
88 genes including KRAB-ZNFs, showing that MORC2 neurodevelopmental disorders are
89 characterized by striking epigenetic changes in cells outside the nervous system.[47] Notably,
90 the functional consequences of removing MORC2 depends substantially on the cellular
91 context. For example, loss of MORC2 in the globally-hypomethylated K562 line causes
92 massive upregulation of young L1 subfamilies, together with changes in KRAB-ZNF
93 expression.[8] In contrast, we recently found that removal of MORC2 in a robustly-methylated
94 neural progenitor cell line had only mild effects on L1 expression – indeed, only when DNA

95 methylation was experimentally removed did MORC2 bind to the activated L1s and dampen
96 their expression.[33] Thus, when young L1 promoters are methylated and silenced, MORC2
97 ignores these sequences and is bound to either older, intronic L1s (transcribed as part of genic
98 pre-mRNA) or other transcribed lineage-specific repeats – in the nervous system, data from
99 our lab and others suggest these to be primarily alpha-satellite repeats and clustered
100 protocadherin genes.[33,34]

101 Together these observations underscore the layered regulation of repeats in somatic cells and
102 suggest critical functions of MORC2 early in development when the genome is relatively
103 hypomethylated. In this study we use a combination of chromatin profiling, long-read DNA
104 methylation analysis and iPSC modelling to demonstrate (i) how ATPase mutations affect the
105 distribution of MORC2 chromatin binding in the neural lineage, and (ii) the critical function of
106 MORC2 chromatin binding in directing CpG methylation patterns over hominoid-specific L1s
107 and repetitive gene clusters in early neurodevelopment. Together our results define the vital
108 role of MORC2 in safeguarding the somatic human genome upon exit of pluripotency by
109 ensuring CpG methylation patterning over repeats in a transcription-dependent manner,
110 analogous to the piRNA pathway in the germline.

111 **RESULTS.**

112 **MORC2 binds to distinct chromatin states in neural cell lines**

113 MORC2 is a potent and avid dsDNA binding protein.[36,37] The prevailing biochemical model is
114 that reversible ATP-dependent dimerization of the N-terminal ATPase module coupled to
115 constitutive C-terminal dimerization via coiled coil domain 3 enables chromatin compaction
116 by trapping DNA between these domains (**Figure 1A)**.[36,39] We first profiled MORC2 chromatin
117 binding using an optimized CUT&RUN (cleavage under targets and release using nuclease)
118 protocol in SHSY5Y cells and embryo-derived human neural progenitor cells (**Figure 1B, Supp**
119 **Fig 1A,B**).[48] In each cell type we clustered MORC2 binding regions by assessing peak shape
120 and co-occupancy with three histone modifications in control cells: H3K9me3, H3K4me3 and
121 H3K27Ac (**Figure 1C**). We observed broad MORC2 peaks in transcriptionally active, H3K9me3-
122 positive regions such as intronic full-length (>6 kb) L1 retrotransposons and 3' exons of
123 expressed zinc finger (ZNF) genes (**Figure 1D, Supp Fig 1C)**. We also observed widespread
124 evidence of MORC2 binding to bivalent chromatin i.e. H3K4me3/H3K27Ac-marked promoters
125 of expressed genes embedded in H3K9me3-positive chromatin, such as clustered ZNF and

126 protocadherin genes. In our hands a minority of narrow MORC2 peaks were identified over
127 gene regulatory elements marked by H3K27Ac and/or H3K4me3 in H3K9me3-negative
128 chromatin contexts. Taken together, in neural cells MORC2 localizes to distinct chromatin
129 states characterized by transcriptional activity and either broad or narrow occupancy,
130 exemplified by L1 retrotransposons and repetitive clustered genes such as ZNFs.

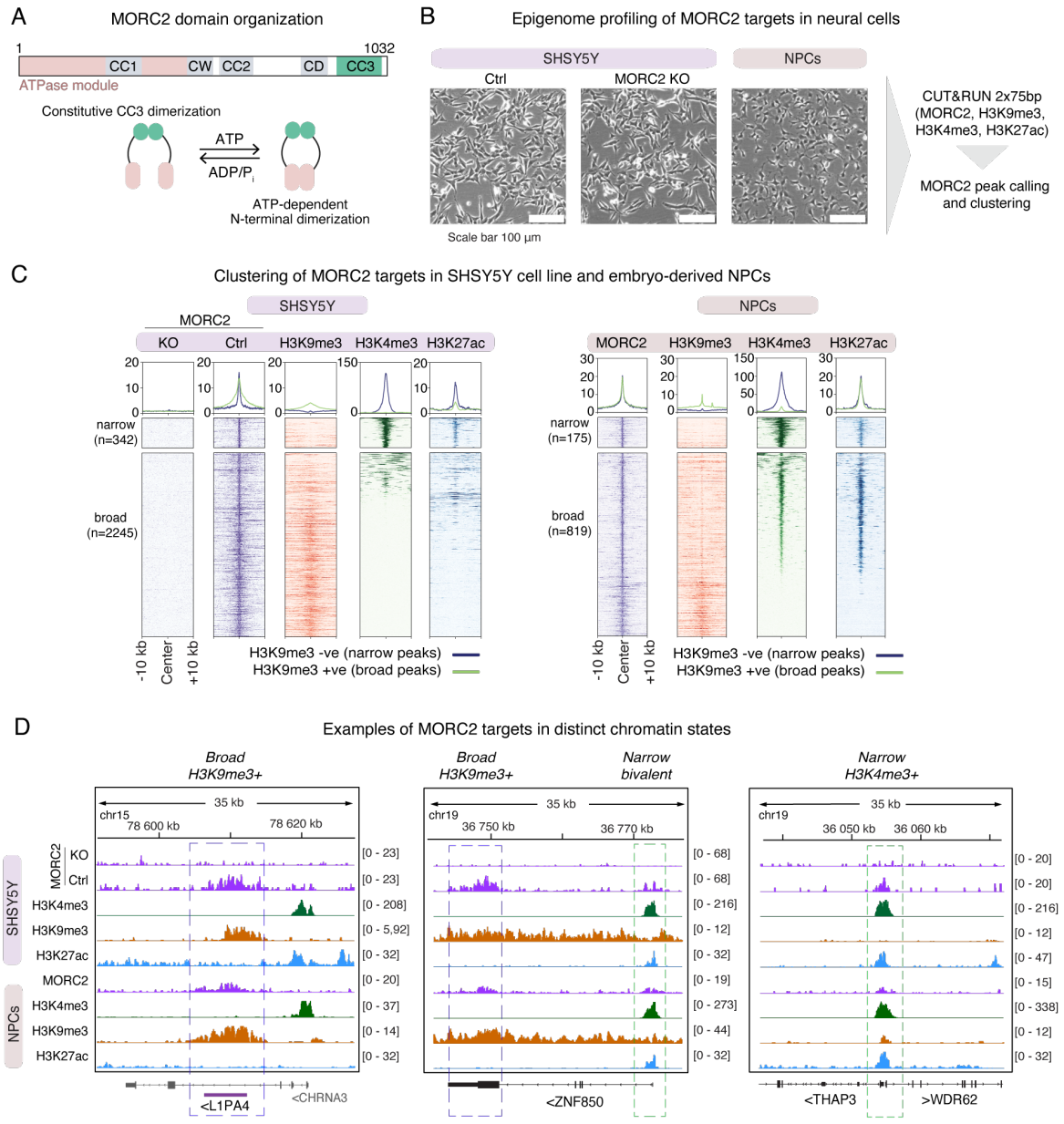

131

132 **Figure 1. MORC2 binds to distinct chromatin states in neural cell lines. (A)** MORC2 domain structure (top) and
133 schematic of ATP-dependent N-terminal dimerization (bottom). **(B)** CUT&RUN workflow for epigenome profiling
134 of SHSY5Y and hNPC cell lines. **(C)** Heatmap illustrating the epigenomic context of distinct MORC2 targets by
135 CUT&RUN signal in SHSY5Y (left) and NPC (right) cell lines with indicated antibodies. Displayed are the genomic
136 regions spanning ± 10 kb from the center. K-means clustering defined H3K9me3-negative, MORC2-narrow peaks
137 (top) and H3K9me3-positive, MORC2-broad peaks (bottom) in each cell type. **(D)** Genome browser tracks
138 showing CUT&RUN enrichment profiles of MORC2 and histone modification over examples MORC2 targets with

139 distinct epigenomic associations. Data are representative of at least two replicates for MORC2, H3K9me3 and
140 H3K4me3 in each line, while H3K27Ac profiling was conducted once in SHSY5Y cells and twice in hNPCs.

141

142 **ATPase dimerization mutants abolish L1 binding and disrupt the balance of MORC2**
143 **chromatin occupancy**

144 Mutations in patients with MORC2 neurodevelopmental disorders all cluster to the N-
145 terminal ATPase module.[46] To interrogate how reversible ATP-dependent dimerization
146 impacts MORC2 chromatin binding we made use of two mutants that we previously found
147 shift this equilibrium in opposite directions: Y18A, a structure-guided mutation that prevents
148 ATPase dimer formation, and S87L, a patient mutation that leads to constitutive ATPase
149 dimerization (**Figure 2A**).[37] We reintroduced HA-tagged proteins to clonal MORC2-KO SHSY5Y
150 cells (**Figure 2B**) and first confirmed that WT, Y18A and S87L MORC2 variants were expressed
151 and nuclear as assessed by Western blotting (**Figure 2C**) and imaging (**Supp Fig 2**). CUT&RUN
152 analysis revealed that both Y18A and S87L variants were completely lost over L1s bound by
153 the WT protein (**Figure 2D,E**). Importantly, these effects were reproducible using antibodies
154 raised against the MORC2 protein itself and its HA epitope tag. Both variants were lost from
155 3' exons of ZNF genes but remained bound to the promoters of those genes, suggesting that
156 ATPase dimerization is not required for promoter occupancy. Notably, the binding of S87L
157 MORC2 to ZNF promoters was reproducibly enhanced relative to WT, suggesting that this
158 mutation causes relocalization of the protein away from L1s and onto gene promoters (**Figure**
159 **2F,G**). Indeed, peak calling revealed a substantially greater overlap of S87L MORC2 with
160 promoters when compared to the WT distribution (**Figure 2H**). Taken together, these results
161 demonstrate that ATPase dimerization mutants disrupt the balance of MORC2 chromatin
162 occupancy. Reversible ATP-dependent dimerization is required for broad MORC2
163 accumulation over L1s but not promoters of target genes (**Figure 2I**). The S87L mutation
164 directs the protein away from L1s and other broad MORC2 targets and increases binding over
165 gene promoters.

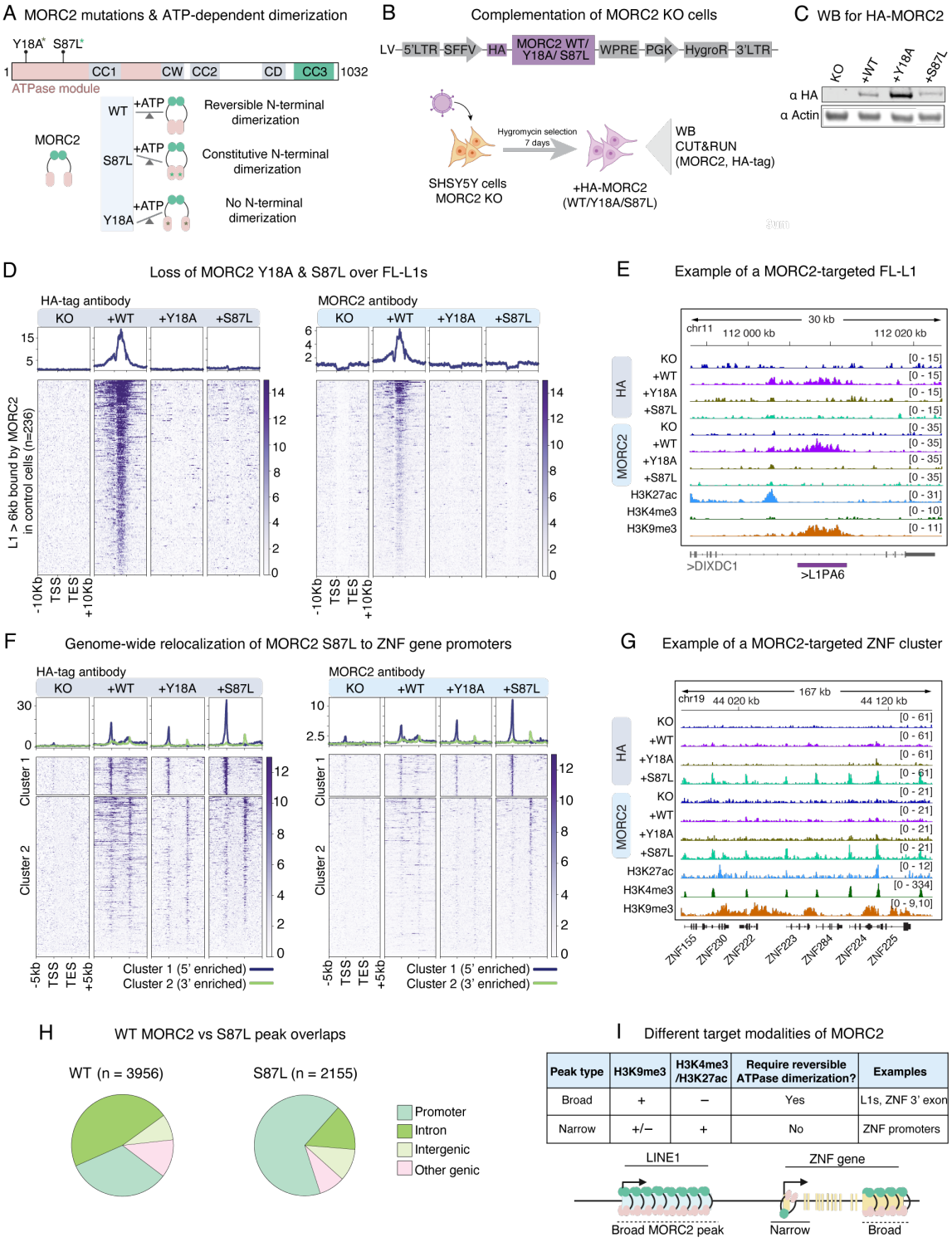

Peak type	H3K9me3	H3K4me3 /H3K27ac	Require reversible ATPase dimerization?	Examples
Broad	+	–	Yes	L1s, ZNF 3' exon
Narrow	+/–	+	No	ZNF promoters

Figure 2. ATPase dimerization mutants abolish L1 binding and disrupt the balance of MORC2 chromatin occupancy. (A) Schematic representation of MORC2 protein domains and the position of ATPase disease mutations (top) and the effect of the mutations on the N-terminal dimerization equilibrium (bottom). **(B)** Schematic workflow of MORC2 complementation experiments and subsequent analyses. **(C)** Western blot validating the expression of complemented HA-tagged MORC2 variants. **(D)** Heatmap showing CUT&RUN enrichment of MORC2 binding over full length (FL, >6 kb) LINE1 elements bound by MORC2 WT in KO and complemented cell lines (+WT MORC2, +Y18A MORC2, +S87L MORC2) as detected using HA-tag antibody (left) and MORC2 antibody (right). Shown are the LINE1 loci scaled to 6 kb with 10 kb up- and down-stream of the elements. Unique mapping was enforced and experiments were repeated at least once with similar results. **(E)**

Genome browser tracks of CUT&RUN enrichment signal for MORC2 binding (KO and complemented cell lines) and histone modifications (H3K27ac, H3K4me3, H3K9me3) over an example LINE1 element. Unique mapping was enforced. **(F)** Heatmap showing CUT&RUN enrichment of MORC2 binding over all ZNF genes (n=503, hg38) in KO and complemented cell lines (+WT MORC2, +Y18A MORC2, +S87L MORC2) as detected using HA-tag antibody (left) and MORC2 antibody (right). Shown are the scaled ZNF genes ± 5 kb. K-means clustering on the S87L MORC2 sample identified 5'-enriched (top) and 3'-enriched (bottom) ZNF genes. **(G)** Genome browser tracks of CUT&RUN enrichment signal for MORC2 binding (KO and complemented cell lines) and histone modifications (H3K27ac, H3K4me3, H3K9me3) over a ZNF gene cluster on chr19. **(H)** Genome overlaps of WT and S87L HA-MORC2 peaks. **(I)** Schematic of the requirements for reversible N-terminal dimerization over different target classes of MORC2. MORC2 accumulation over broad peaks is found over regions enriched in H3K9me3 signal, such as LINE1s and ZNF 3´exons, and requires reversible N-terminal dimerization. Narrow MORC2 binding to gene regulatory elements such as ZNF gene promoters is found in regions enriched in H3K4me3 and H3K27ac signal, and does not require reversible N-terminal dimerization.

MORC2 ATPase mutations cause loss of L1 silencing and ZNF hyperrepression in iPSCs

Next we sought to explore the functional impact of these observations on transcriptional regulation in a relevant developmental cell model. We used CRISPR editing to derive induced pluripotent stem cell (iPSC) clones bearing the S87L mutation described above and a second ATPase mutation, E27K, which also causes a severe neurodevelopmental phenotype and would be predicted to similarly disrupt ATPase activity based on its structural position at the N-terminal ATP-induced dimerization interface.[37,46] We note here that though patients carry heterozygous mutations, our study sought to provide mechanistic insight into how ATPase mutations affect MORC2 function over a developmental timecourse and as such we induced homozygous *MORC2* editing (**Figure 3A, Supp Fig 3A**). We subjected unedited controls to the same clonal expansion procedures and confirmed that each iPSC clone expressed pluripotency markers and that the copy number and genomic integrity at predicted off-targets was not affected by the editing (**Figure 3B, Supp Fig 3B,C**). Transcriptomic analysis using paired-end (150x150-bp) polyA+ RNA sequencing (RNA-seq) showed that the patient mutations both cause significant derepression of evolutionarily-young, hominoid-specific L1 subfamilies, with the S87L mutation having a more pronounced effect (**Figure 3C, D**). CUT&RUN profiling of the H3K4me3 mark mapped to individual full-length L1 elements provided orthogonal validation of young L1 expression **(Figure 3E)**. In line with chromatin binding data above illustrating complete loss of L1 binding, the S87L mutation caused L1 transcriptional activation at comparable levels to a loss of function control in which we used a validated CRISPRi vector [33] to robustly knock down MORC2 expression in iPSCs (**Figure 3E, Supp. Fig 3D-G**). L1 derepression was further confirmed in Western blots and immunofluorescence experiments as measured by L1-encoded protein orf1p in the mutant

213 and CRISPRi conditions relative to controls (**Figure 3F, Supp Fig 3H**). We also observed
214 pronounced derepression of L1 fusion genes where evolutionarily-young L1s act as alternative
215 promoters (**Supp Fig 4A**). Several of these genes have documented or predicted functions in
216 the brain. For example, *GABRR1*, whose promoter is shared with a L1PA2 element, encodes a
217 key factor involved in GABAergic neurotransmission in the central nervous system[49] and
218 *DYNC1I1*, which contains an intronic L1PA3, encodes a neuron-enriched dynein intermediate
219 chain (**Supp Fig 4B**). Notably, and in line with the chromatin binding data, alongside L1 loss of
220 function we observed simultaneous hyperrepression of zinc finger genes in E27K (n=22), S87L
221 (n=11) or both (n=19) MORC2 mutants (log2 fold-change < -2, padj < 0.05, DESeq2) (**Figure**
222 **3G,H**). This effect was a gain of function associated with the S87L and E27K mutants that was
223 not observed in the MORC2-CRISPRi cells. Taken together these data show how MORC2
224 ATPase mutations change the dynamics of chromatin target engagement, leading to both loss
225 and gain of function effects on transcriptional control of its distinct targets.

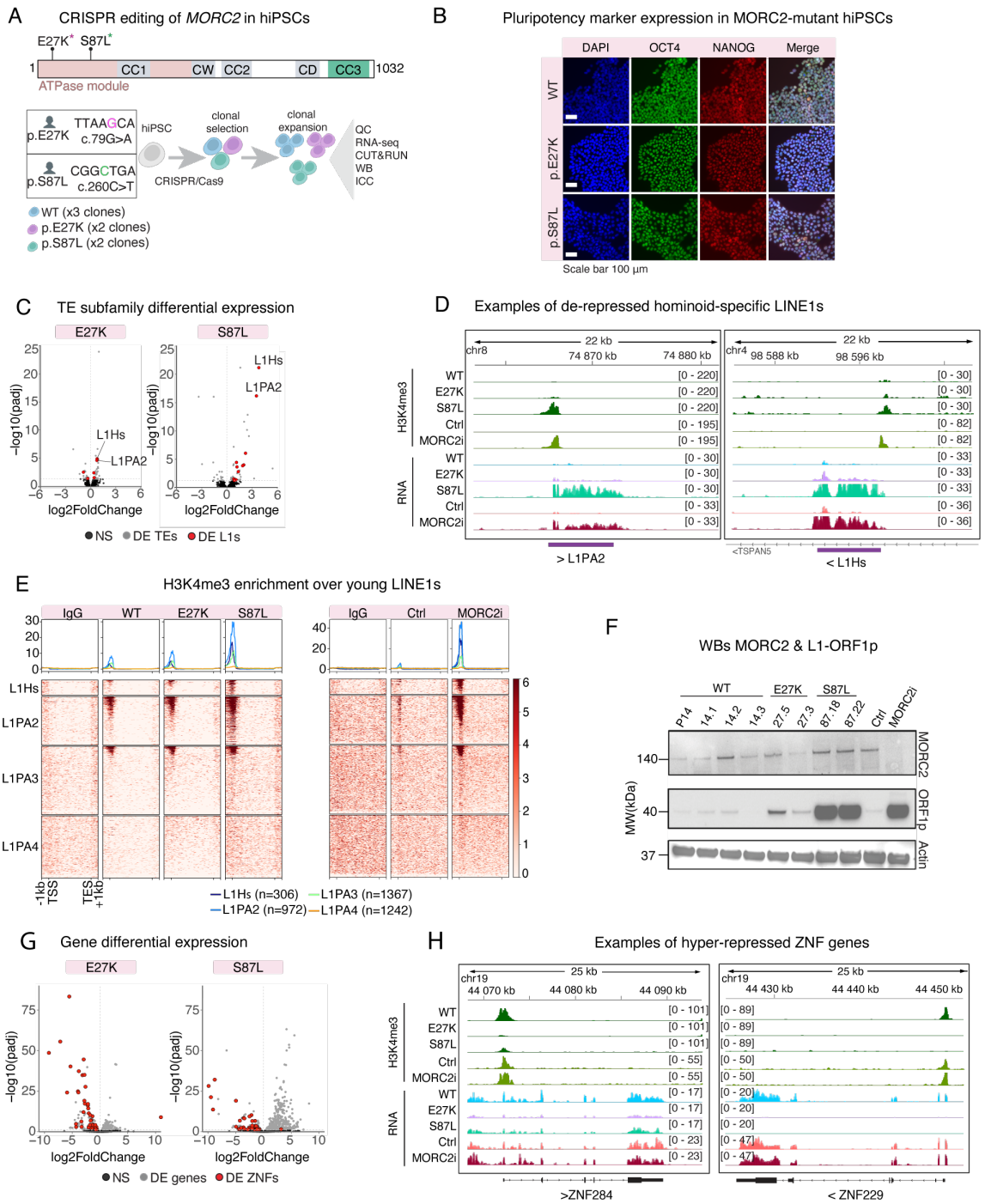

Figure 3. MORC2 ATPase mutations cause loss of L1 silencing and ZNF hyperrepression in iPSCs. (A) Schematic of CRISPR editing and subsequent analyses. Induced homozygous mutations were c79G>A and c260C>T for E27K and S87L mutants, respectively. **(B)** Immunocytochemestry of pluripotency markers (NANOG, OCT4, SOX2) for a representative hiPSC clone of each MORC2 genotype. **(C)** Volcano plot showing the results of the differential expression analysis (DESeq2) on a TE subfamily level using TEtranscripts. Differentially expressed LINE1 subfamilies are highlighted in red, other differentially expressed subfamilies are presented in grey (log2FoldChange $\neq 0$, padj <0.05). Two experimental replicates per clone were sequenced and data from each clone pooled prior to differential analysis (n=4 WT vs n=4 E27K vs n=4 S87L). **(D)** Genome browser tracks showing H3K4me3 and bulk RNA-seq data over two example loci of derepressed hominoid-specific full-length L1s. Unique mapping was enforced for all data over individual loci. Also shown are representative data from MORC2 CRISPRi

(n=3) and Control (n=3) hiPSCs, see also Supp Fig 3. **(E)** Heatmap of the CUT&RUN signal enrichment of H3K4me3 and non-targeting IgG controls over reference L1 insertions belonging to the evolutionarily-youngest subfamilies (L1HS, L1PA2-4) in MORC2 mutant and CRISPRi cell lines. For each WT and mutant cell line, cells from two clones were pooled prior to CUT&RUN, which was conducted at least twice with similar results. Experiments with control and MORC2 CRISPRi cells were repeated twice with similar results. Unique mapping was enforced for CUT&RUN data shown. **(F)** Western Blot showing expression of MORC2 and of L1 ORF1p in MORC2 mutant and CRISPRi cell lines. The experiment was repeated once with similar results. **(G)** Volcano plot showing the results of the differential gene expression analysis (DESeq2). Differentially expressed ZNF genes are highlighted in red, other differentially expressed genes are presented in grey (padj <0.05). Two experimental replicates per clone were sequenced and data from each clone pooled prior to differential analysis (n=4 WT vs n=4 E27K vs n=4 S87L). **(H)** Genome browser tracks showing H3K4me3 and bulk RNA-seq data over example loci of two hyperrepressed ZNF genes. Unique mapping was enforced for all data over individual loci. Also shown are data from MORC2 CRISPRi (n=3) and Control (n=3) hiPSCs, see also Supp Fig 3.

Transcriptional phenotypes of MORC2 mislocalization persist upon neural differentiation

To model how these transcriptional phenotypes change upon exit from pluripotency and neural differentiation, we set out to differentiate the iPSC lines to neural progenitor cells (NPCs). Using a previously-described 2D NPC differentiation protocol[50] we observed widespread cell death in the MORC2-CRISPRi and S87L lines, precluding further analysis. As an alternative we made use of an undirected 15-day cerebral organoid protocol as a model for human brain development in 3D (**Figure 4A**). At this timepoint our previous data showed that organoids are largely composed of NPCs, enabling detailed analysis of L1 and gene regulation in bulk.[28] 3D differentiation indeed improved cell survival and cells bearing both MORC2 mutations or carrying the MORC2 CRISPRi lentiviral vector could form characteristic neural rosettes after 15 days (**Figure 4B**). Single nucleus RNA sequencing confirmed that NPCs and early neurons constituted the major cell populations in these preparations across multiple batches and clones (**Supp Fig 4A-D**). Differential expression analysis on day-15 organoids from at least two clones and three experimental batches showed that the transcriptional phenotype observed in hiPSCs – that is, L1 derepression in mutant and CRISPRi lines and ZNF hyperrepression specifically in the mutants – persisted upon differentiation (**Figure 4C-G**). We found that the promoters of young L1 integrants identified to be derepressed in hiPSCs were highly enriched with the H3K4me3 active mark in MORC2-S87L and MORC2-CRISPRi day 15 organoids (**Figure 4F**). We also observed upregulation of lineage-specific clustered protocadherin genes in MORC2 mutant organoids, while this effect was stronger in MORC2-CRISPRi samples (**Supp Fig 5A,B**). Taken together, our data illustrate that

the transcriptional phenotypes of MORC2 targets in the pluripotent state persist upon exit from pluripotency and early neurodevelopment.

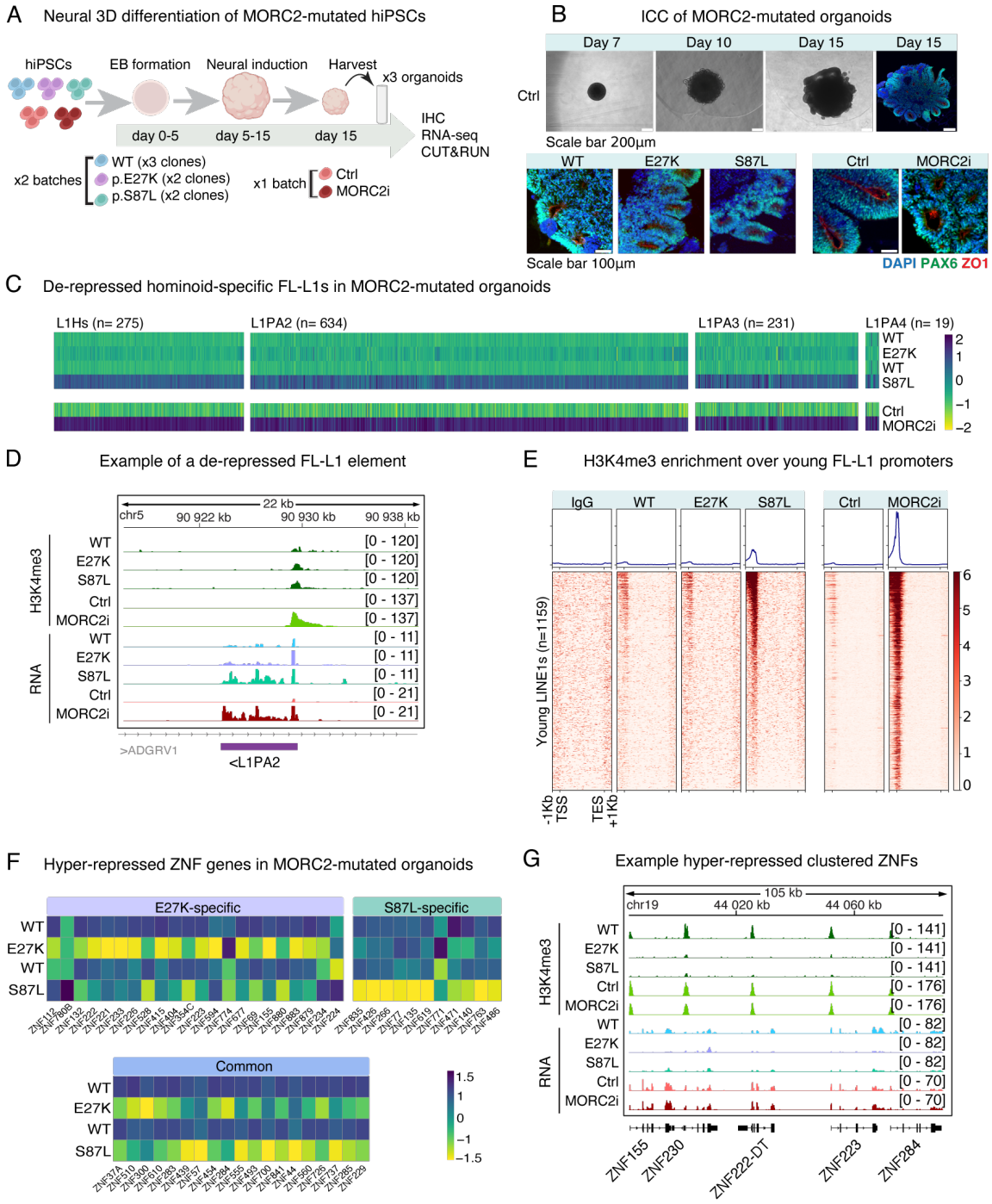

Figure 4. Transcriptional phenotypes of MORC2 mislocalization persist upon neural differentiation. (A) Schematic of differentiation of MORC2 mutant and CRISPRi cell lines from hiPSCs to cerebral organoids. Two batches of organoids were produced for both S87L and E27K clones and three for WT clones. One batch was produced for MORC2 CRISPRi and its corresponding control cell line in which hiPSCs were transduced with a non-targeting lentiviral CRISPRi vector. **(B)** Representative bright field images and immunohistochemistry of cerebral organoid formation in a control line at different time points (top). Immunohistochemistry of PAX6 (green) and ZO1 (red) in day 15 organoid sections (bottom). **(C)** Scaled heatmap showing the normalized read counts of individual full length (FL) LINE1 from youngest subfamilies (L1HS, L1PA2-4) that had been derepressed in MORC2 E27K and S87L mutant and MORC2 CRISPRi hiPSCs (log2FoldChange >0, padj <0.05). Data are representative of

three replicates of two clone across two batches (n=9 WT vs n=9 E27K vs n=9 S87L). Unique mapping was enforced. **(D)** Genome browser tracks showing CUT&RUN H3K4me3 enrichment and bulk RNA-seq data over an example derepressed full-length L1. Unique mapping was enforced. **(E)** Heatmap of the CUT&RUN signal enrichment of H3K4me3 and non-targeting IgG control over reference full-length L1 insertions belonging to the to the youngest subfamilies (L1HS, L1PA2-4) that were expressed in MORC2 mutants and CRISPRi hiPSCs. For WT and mutant genotypes, organoids from two clones were pooled prior to CUT&RUN, which was conducted at least twice with similar results. Unique mapping was enforced **(F)** Scaled heatmap showing the normalized read counts over ZNF genes hyperrepressed in MORC2 E27K and S87L mutants hiPSCs (log2FoldChange <0, padj <0.05). **(G)** Genome browser tracks showing CUT&RUN H3K4me3 enrichment and bulk RNA-seq data over a hyper-repressed ZNF cluster on chr19. Unique mapping was enforced.

MORC2 directs CpG methylation patterning over the repetitive human genome

As the observed transcriptional phenotypes persisted from the pluripotent state to day-15 organoids, we hypothesized a defect in CpG methylation patterning over MORC2 targets. To investigate methylation changes over MORC2-targeted repetitive elements we used whole-genome Oxford Nanopore long-read sequencing (**Figure 5A**). While genome-wide methylation was robust and stable across all conditions (**Figure 5B**), the S87L mutation in MORC2 caused a catastrophic methylation loss over the promoter of the youngest L1Hs and L1PA2 integrants (**Figure 5C-E**). Loss of methylation over young L1 promoters was mirrored in the MORC2-CRISPRi organoids and across organoid preparations derived from independent clones, confirming the effect over these targets was reproducible and a direct loss of function effect (**Figure 5C-E, Supp Fig 6A**). Leveraging the Nanopore data to call polymorphic L1 insertions absent from the hg38 reference, we also observed striking loss of methylation over these youngest copies in both genetic backgrounds tested (**Supp Fig 6B**). Importantly, we found that the effect was most striking to the L1 elements transcribed in the pluripotent state, illustrating a transcription dependence of the methylation patterning directed by MORC2 (**Figure 5F**). We also observed hypermethylation over zinc finger gene clusters that were specific to the MORC2 mutant but not CRISPRi organoids – in particular over the promoter of the ZNF genes hyperrepressed in pluripotent cells **(Figure 5G,H).** As major alterations of the methylation are present across the ZNF gene clusters (**Supp Fig 6C**), including gene bodies, we speculate that this could be driven by effects on 3D chromatin structure in MORC2 mutant cells, though this remains to be tested systematically. Together our observations demonstrate the critical role of MORC2 in directing CpG methylation patterning over its repetitive targets upon exit of pluripotency and early neurodevelopment.

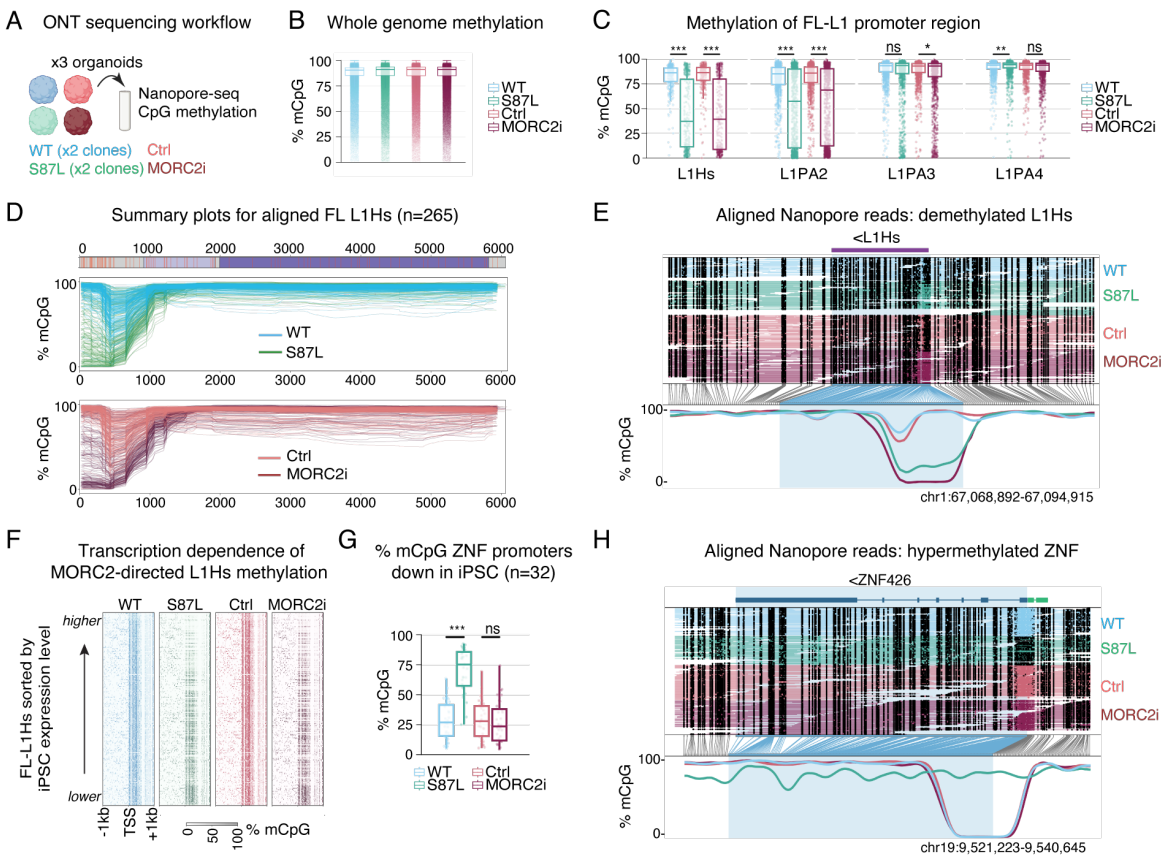

Figure 5. MORC2 directs CpG methylation patterning over the repetitive human genome. (A) Schematic of DNA methylation analysis workflow. For each clone and cell line, DNA from three organoids was extracted and pooled for Oxford Nanopore sequencing (ONT). **(B)** Boxplots showing the CpG methylation levels across the whole genome and **(C)** over the first 900-bp of full length (FL) evolutionary young LINE1 elements (L1HS, L1PA2-4), which corresponds to the 5' UTR promoter region. P-value as calculated by a two-sided Wilcoxon rank sum test with continuity correction (p-values adjusted following Benjamini–Hochberg correction). **(D)** Composite plot showing CpG methylation levels of all reference FL-L1HS elements greater than 6 kb (hg38) over the entire element in the given conditions. **(E)** Aligned Nanopore reads showing loss of CpG methylation over the promoter of an example L1HS locus in S87L and MORC2i organoids. Methylated and non-methylated CpGs are represented by filled black circles and open (coloured) circles, respectively. **(F)** Heatmap showing the CpG methylation level over the promoter of FL-L1HS, sorted by expression level in hiPSC S87L mutants as assessed by promoter H3K4me3 level. Methylation changes are anti-correlated to their expression in hiPSCs. **(G)** CpG methylation level of the promoter of ZNF genes downregulated in MORC2-mutant iPSCs. **(H)** Aligned Nanopore reads showing hypermethylation over the promoter and general methylation alteration over the body of a hyperrepressed ZNF gene. ns, non-significant; *, p–value < 0.05; **, p–value < 0.01; ***, p–value < 0.001.

DISCUSSION.

In this study we report and relate two key mechanistic insights on the role of the MORC2 ATPase in epigenetic reprogramming of the repetitive genome. First, we find that reversible ATP-dependent dimerization is required for broad MORC2 accumulation over L1 retrotransposons, but not required for its binding to gene promoters, and that mutation of the ATPase module titrates MORC2 occupancy between these target classes. Second, we find

342 that MORC2 chromatin binding directs CpG methylation patterns over its targets upon exit of
343 pluripotency and early human neurodevelopment. The model is summarized in **Figure 6**.

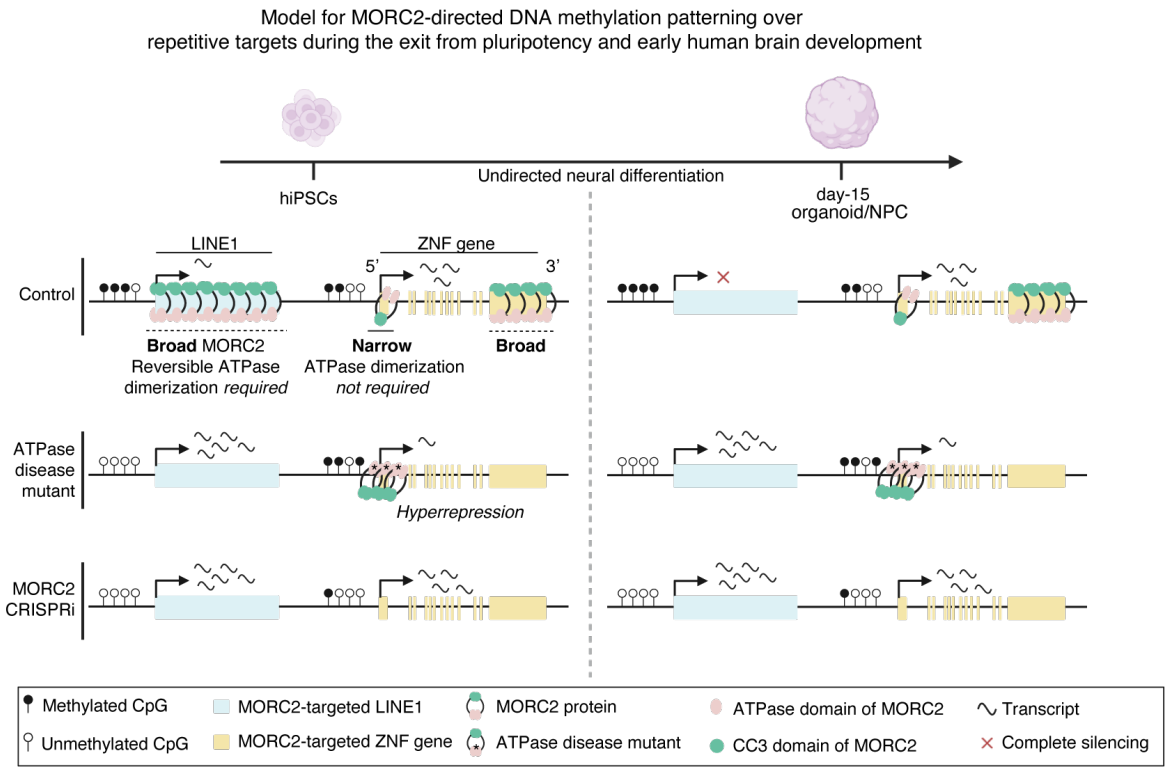

344

345 **Figure 6.** Model for MORC2-directed CpG methylation patterning over repetitive targets during the exit from
346 pluripotency and early human brain development.

347

348 The physiological relevance of MORC2 ATP-dependent dimerization is evident from clinical
349 genetics reports over the past ten years, where missense mutations in patients with severe
350 neurodevelopmental disorders all map to the ATPase module.[45–47] Our previous biochemical
351 and structural studies identified that these mutations change the ATPase activity and
352 dimerization dynamics of the purified protein,[37] and here we provide a framework to explain
353 how this translates at the level of chromatin binding. MORC2 has two main chromatin binding
354 modes – broad accumulation over H3K9me3-marked sites, and narrow binding to gene
355 regulatory elements marked by H3K4me3/H3K27Ac.[32] When reversible ATP-dependent
356 dimerization is perturbed by mutation of the ATPase module, MORC2 fails to accumulate over
357 broad sites but binding is maintained or enhanced at narrow sites. Crucially, mutations that
358 shift the equilibrium of N-terminal dimerization in either direction cause loss of function over
359 L1s – supporting the notion that the lifetime of ATP-dependent MORC dimers is a critical

360 parameter in driving chromatinization of certain targets.[36,37,39] The observation that binding
361 of MORC2 mutants to gene promoters is maintained or enhanced explains the hyper-
362 repression phenotype observed in engineered cell lines or patient samples,[32,47] and in the
363 stem cell models of early brain development that we characterize here. That many of the
364 genes hyperrepressed in MORC2 mutant cells encode KRAB-ZNFs, themselves associated with
365 epigenetic TE silencing, highlights the central and multifaceted role of MORC2 in TE biology.
366 Many of the hyperrepressed ZNFs in MORC2 mutant lines are transcription factors or
367 repressors that each target hundreds of genomic locations, illustrating enormous potential
368 for pleiotropic, indirect effects on chromatin and transcription of disrupting the balance of
369 MORC2 chromatin binding sites via ATPase mutation. These complex gene regulatory
370 networks require further investigation, but our data suggest that TE transcription and TE-
371 induced chromatin structure are likely important molecular phenotypes to consider in
372 patients with MORC2 disorders.

373 Work by us and others has established that the HUSH-MORC2 corepressor targets transcribed
374 and relatively hypomethylated repeats with little apparent preference for particular DNA
375 sequence motifs.[8,33,51,52] The prevailing model is that the complex is recruited to long,
376 intronless units with some A-rich bias in the sense strand.[51] In human pluripotent stem cells,
377 the primary targets of MORC2 are the hominoid-specific LINE-1 retrotransposons that we
378 recently reported to be transcribed and relatively hypomethylated at steady-state.[28] This is
379 likely the critical way that the HUSH-MORC2 axis preserves genome stability in early
380 development: a subset of the youngest L1s remain competent for autonomous transposition
381 and their encoded proteins provide the molecular apparatus for mobilization of other TEs.
382 Transcription-dependent TE targeting is in contrast to the KRAB-ZNF/TRIM28 pathway, which
383 is recruited to particular DNA sequence motifs in repeats via rapidly-evolving ZNF domains.[22–
384 26] Such complementary modes of targeting help explain why HUSH-MORC2 and KRAB-ZNFs
385 may regulate overlapping yet distinct sets of genomic repeats and genes in different cellular
386 contexts.[30,35] The situation at the youngest human L1s is of particular interest: while
387 numerous KRAB-ZNFs (and TRIM28) are competent to bind L1HS and L1PA2 subfamilies
388 through conserved sequences in the L1 ORFs,[24,25] deletion of 129 bp in the ancestral L1PA3
389 promoter region within the ZNF93 binding site may have evaded promoter methylation by
390 this factor in evolutionarily-younger copies.[26,27] Our data supports the idea that the HUSH-

391 MORC2 corepressor is recruited to these youngest, transcriptionally-active elements for
392 which a new KRAB-ZNF has yet to evolve.[51]

393 The interplay of these epigenetic silencing systems is of particular interest in early
394 development, when methylation patterns of the germline are globally erased and re-
395 established.[12] The KRAB-ZNF/TRIM28 system is thought to protect against erasure of germline
396 methylation at certain targets: for example, ZFP57 and ZFP445 bind DNA sequences at
397 imprinting control regions, recruiting TRIM28 and DNMTs to maintain methylation at paternal
398 or maternal imprints.[53,54] Many TEs are also resistant to demethylation, but it is thought the
399 youngest human L1s are demethylated early post-fertilization, maintaining relative
400 hypomethylation throughout pre-implantation development.[27] Although our primed iPSC
401 models reflect a post-implantation developmental stage, we note that *MORC2* is also robustly
402 expressed in the pre-implantation human embryo[55] and our data suggest that the protein is
403 a key factor that directs methylation over these youngest L1 copies. Whether MORC2 protects
404 against erasure of germline methylation or promotes re-establishment of human L1
405 methylation following erasure is challenging to answer, but the transcription-dependence of
406 HUSH-MORC2 recruitment to L1s strongly favours a reestablishment model. Nevertheless,
407 the underlying mechanism and timing of human L1 promoter methylation warrants further
408 investigation and it would be exciting to leverage new blastoid models in this effort.[56]

409 Taken together, our study reveals how ATP-dependent dimerization of MORC2 is coupled to
410 chromatin binding and DNA methylation patterning. The precise sequence of how
411 establishment and/or maintenance DNA methyltransferases (DNMTs) are recruited to
412 MORC2 targets in early development remains an interesting open question. MORC2-driven
413 chromatin compaction is known to correlate with H3K9me3 deposition at certain sites,[8,32,33]
414 which may in turn recruit maintenance methyltransferase DNMT1.[57,58] However, since
415 aberrant MORC2 mutant binding to certain (H3K9me3-negative) gene promoters also results
416 in promoter hypermethylation, we suggest that MORC2 may be directly involved in licensing
417 DNA methylation its target sites. This is somewhat reminiscent of a recent study in mouse
418 gonocytes where Morc1, a germline-restricted TE repressor,[59] was suggested to make distinct
419 complexes leading to piRNA-directed H3K9me3 and DNA methylation at different TEs.[60] Our
420 data reinforce the model that the transcriptional activity of a locus determines its sensitivity
421 to MORC2 binding and, we show here, targeted CpG methylation upon differentiation. Such

422 a model could explain how the transcription factor yin-yang 1 (YY1) functions as both
423 activator[61] and repressor[31] of human L1s: YY1 drive transcription initiation of these young
424 elements in the pluripotent state, which marks the locus for MORC2-directed methylation. It
425 is also noteworthy that certain young L1s are demethylated and transcriptionally-active in
426 both organoids and human brain tissue.[3,28,31] Further work is required to determine how
427 MORC2-directed methylation may be avoided over these elements – or whether the elements
428 are subject to active demethylation upon neural differentiation. How the mechanisms we
429 describe here play out in terminally differentiated cells such as neurons also promises to be a
430 fruitful area of research.

431 **METHODS.**

432 **Cell culture.**

433 *hiPSCs.* Two human iPSC lines were used in this study: Ctrl-14 hiPSCs, which were
434 reprogrammed by the Cell and Gene Therapy Core at Lund Stem Cell Center from human
435 fibroblasts via mRNA mediated reprogramming as described elsewhere,[62] and a
436 commercially-available line from RIKEN (RBRC-HPS0328 606A1). hiPSCs were cultured based
437 on previously developed protocols.[50,63] Briefly, cells were maintained in multi-well plates
438 coated with Biolaminin 521 (0.7 mg cm^{-2}), and fed daily with StemMACS iPS-Brew XF
439 containing 0.5% penicillin–streptomycin (Gibco). hiPSCs were passaged upon reaching 70-
440 80% confluency. Firstly, cells were rinsed with DPBS (Gibco), dissociated using Accutase
441 (Gibco) for 5-7 min at 37°C then washed off by DMEM-F12 (Gibco) and KnockOut Serum
442 Replacement (KSR) (Gibco) and centrifuged at 400g for 5 min. Rock inhibitor (10 uM, Miltenyi)
443 was added to the media following cell thawing, lentiviral transduction, FACS and CUT&RUN
444 experiments.

445 *SH-SY5Y cells.* SH-SY5Y human neuroblastoma cells (ATCC CRL-2266) were a gift from Harvey
446 McMahon (MRC-LMB). Cells were cultured in flasks and fed every 3-4 days with complete
447 culture medium containing DMEM-F12, 10% FBS, MEM non-essential amino acids solution
448 and 1x penicillin/streptomycin (Gibco). When 80% confluent, cells were rinsed with DPBS
449 (Gibco), incubated with trypsin (Gibco) for 5-7 minutes at 37°C to detach, and washed off with
450 the media to quench the enzyme. To maintain a Mycoplasma-free culture, cells were routinely
451 tested and returned negative.

452 *Human unguided cerebral organoids culture*. Human cerebral brain organoids were generated
453 using the STEMdiff Cerebral organoid kit (Stem Cell Technologies) following the
454 manufacturer's instructions and based on a previously established protocol.[64] First, embryoid
455 bodies (EB) were generated following disassociation and resuspension of hiPSCs in EB seeding
456 medium (STEMdiff™ Cerebral Organoids Basal Medium 1 and STEMdiff™ Cerebral Organoids
457 Supplement A, supplemented with 10 μM of Y-27632) in round bottom ultra-low attachment
458 96-well plates. On day 5, to avoid EB fusion individual EBs were distributed into single wells
459 of ultra-low attachment 24-well plates and incubated with Induction Medium (STEMdiff™
460 Cerebral Organoids Basal Medium 1 and STEMdiff™ Cerebral Organoids Supplement B) for
461 48 h at 37°C. On day 7, organoids were then embedded into Matrigel (Stem Sell Technologies)
462 and cultured in ultra-low attachment 6-well plates (10-12 organoids/well) with Expansion
463 medium (STEMdiff™ Cerebral Organoids Basal Medium 2, STEMdiff™ Cerebral Organoids
464 Supplement C, STEMdiff™ Cerebral Organoids Supplement D). Up until day 15, organoids
465 were fed twice (on day 10 &13) with Maturation media (STEMdiff™ Cerebral Organoids Basal
466 Medium 2, STEMdiff™ Cerebral Organoids Supplement E). Organoids were harvested on day
467 15 for downstream analysis such as bulk RNA-seq (3 snap-frozen organoids per replicate),
468 snRNA-seq (4-5 organoids per replicate), whole genome Oxford Nanopore sequencing (3-4
469 organoids per replicate), immunostaining (3-4 organoids) and CUT&RUN (3-4 organoids per
470 replicate).
471
472 **Lentiviral vectors.**
473 Lentiviral vectors were produced according to a standard protocol described previously.[65]
474 Briefly, HEK293T cells with a confluency of ~80% were co-transfected with three packaging
475 plasmids (pMDL, psRev, and pMD2G) and the relevant transfer plasmid using
476 polyethyleneimine (PEI; Polysciences), in DPBS. Cell culture media containing lentiviral
477 particles was harvested 48 h after transfection, filtered, and centrifuged at 25,000xg for 1.5h
478 at 4 °C. After removing the supernatant, pellets were gently resuspended in cold PBS and
479 incubated overnight at 4°C. Finally, the lentivirus was aliquoted and stored at -80 °C until use.
480 Lentiviral titration was determined using qPCR targeting the viral WPRE sequence and
481 comparison to a reference virus batch with known titre.
482
483 **CRISPR approaches.**

484 *CRISPR KO.* To generate MORC2 KO SHSY5Y cells two sgRNA were cloned into pSpCas9(BB)-
485 2A-Puro vector (Addgene #48139). sg21 (GGGATCAATATAGAGCACAG) targets exon 9 and
486 sg22 (GCGGACATTAGAAGTACGCCT) exon 11 of *MORC2*. 8 mg of the plasmids was
487 electroporated into $2x10^6$ cells using 100ul tips from Neon electroporation system and placed
488 into 25 cm flasks. After 24 h, 4 mg/mL of puromycin was added to select for electroporated
489 cells. After 10 days single cells were sorted into 96-well plates. Chosen clones were first
490 analysed for the presence of the MORC2 band using Western blotting. Cells were lysed for 30
491 min at 4°C in buffer containing 300 mM NaCl, 100 mM Tris pH 8.0, 0.2 mM EDTA, 0.1% NP40,
492 10% glycerol supplemented with protease inhibitors. Lysates were cleared by centrifugation
493 and supernatant was used for Western blotting using MORC2 (anti-rabbit MORC2, Bethyl),
494 HA (Mouse HA11 901501, Biolegend) and actin antibodies (Mouse α-β-actin, ab8226).
495 DyLight-680 or 800-conjugated secondary antibodies (Thermo Fisher Scientific) were used at
496 1:10,000 dilution and blots were imaged on the Odyssey near-infrared system (LI-COR).
497 Following isolation of genomic DNA (Qiagen), the knockout was confirmed using Sanger
498 sequencing and TIDE analysis.
499 *CRISPR-editing.* To introduce MORC2 S87L and E27K mutations in Ctrl-14 hiPSCs, HiFi Cas9v3,
500 relevant gRNAs and desired sequences to target the MORC2 gene were delivered to cells as
501 Ribonucleoprotein (RNP) and single-stranded oligodeoxynucleotide (ssODN) via
502 nucleofection (P3 Primary Cell 4D-Nucleofector X Kit, Lonza) (**Table 1**). CRISPR editing
503 efficiency was estimated in bulk using genomic PCR and restriction enzyme digestion followed
504 by clonal expansion. Individual clones were collected and primarily tested for the presence of
505 the edit using genomic PCR and restriction enzyme digestion followed by Sanger sequencing.
506 The selected clones with the desired edits underwent karyotyping and sequencing of the 5
507 top-predicted off-targets. Once these quality controls were passed, immunostaining of
508 pluripotency markers OCT4, NANOG and SOX2 was performed on selected clones.
509

Genotype	gRNA	ssODN	hiPSC clone numbers
WT	-	-	P14, 14.1, 14.2, 14.3
MORC2 E27K	ACCAAACAAGAATTCGTGAG	TTATCAACCAGTTCAGCAAGGGCACCAA ACAAGAATTTGTGAGTGGTTCTGAAATG ATAAATACTAAAAGTCAGCAAAAG	27.3, 27.5
MORC2 S87L	CTTCCCAAACTGGATCACAC	GACTCAGGTGTTCGCTTGGCCAACTTCC CAAACTGGATCACACTAGCAGCATCACC TGAAAGGGCAGA CACAAGAGAAAG	87.18, 87.22

510 **Table 1. CRISPR editing of *MORC2*.**

511

512 *CRISPR interference*. A previously-described protocol for CRISPR interference was used to
513 silence *MORC2* transcription in hiPSCs.[66] gRNAs (**Table 2**) were cloned into a dCas9-KRAB-T2A-
514 GFP lentiviral backbone containing both the gRNA under the U6 promoter and dCas9-KRAB-
515 T2A-GFP under the Ubiquitin C promoter (pLV hU6-sgRNA hUbC-dCas9-KRAB-T2a-GFP) using
516 annealed oligos and the BsmBI cloning site. An identical CRISPRi vector containing a gRNA
517 sequence absent from the human genome (LacZ) was used as a non-targeting control. hiPSCs
518 were transduced with MOI 5 and GFP-positive cells were sorted using FACS (FACSAria, BD
519 sciences) on day 10 at 10°C. Sorted cells were centrifuged at 400x*g* for 7 min and pellets were
520 snap frozen on dry ice and kept at −80°C for downstream analysis, or maintained in culture.

521

CRISPRi gRNA target	20-bp targeting sequence (5'-3')
LacZ non-targeting control	TGCGAATACGCCCACGCGAT
MORC2	GCTTCCAAGGACCGGATCGA

522 **Table 2. CRISPRi gRNA sequences.**

523

524 **RT-qPCR.**

525 RT-qPCR was used to check the efficiency of MORC2 CRISPRi. 500 ng RNA was extracted from
526 hiPSCs and used for reverse transcription to generate cDNA with random hexamer primers
527 and the Superscript III reverse transcriptase (Invitrogen). RT-qPCR was performed using SYBR
528 Green I master (Roche) on a LightCycler 480 instrument (Roche). Data were analysed with the
529 ΔΔCt method normalized to housekeeping gene *ACTB*. Primer sequences are given below.

Target	Forward (5'-3')	Reverse (5'-3')
MORC2	ACATGAAGACGCAGGAAGAG	ACTTCCAAGGGCAATTTCTT
ActB	CCTTGCACATGCCGGAG	GCACAGAGCCTCGCCTT

530 **Table 3. RT-qPCR primer sequences.**

531

532 **Lentiviral expression of HA-MORC2 variants.**

533 To express WT and mutant versions of MORC2 on the SHSY5Y MORC2-KO background, we
534 cloned MORC2 into the lentiviral pHRSIN-pSFFV-WPRE-pPGK-Hygro vector (a gift from Paul
535 Lehner, University of Cambridge) with an N-terminal HA-tag. For lentiviral production 293T
536 cells were co-transfected with lentiviral MORC2 vector, pCMVΔR8.91 and pMD.G using the
537 TransIT-293 transfection reagent (Mirus). Supernatants were collected two days post-

538 transfection and cleared by filtering through 0.45 mm membranes. $1x10^6$ of cells were
539 transduced by centrifugation for 90 min at 1000xg in the presence of 300 μL lentivirus-
540 containing supernatant and 5 μg/mL of polybrene. The following day, cells were transferred
541 into 10cm dishes and hygromycin at 400 μg/mL added for selection.
542
543 **Quantitative genotyping qPCR.**
544 Quantitative genotyping PCR (qgPCR) was performed to rule out unintended CRISPR-induced
545 on-target effects (onTEs) at the edited sites. We followed the protocol described in Weisheit
546 et al., 2021.[67] In brief, genomic DNA was extracted from iPSC cells using the DNeasy Blood &
547 Tissue kit (QIAGEN). IDTPrimerQuest was used to design primer pairs to amplify the regions
548 surrounding the edits and FAM-labeled target-specific probes and purchased from IDT (see
549 **Table 4**). We use the TERT Taqman Copy Number Reference assay (Thermo Fisher Scientific)
550 labeled with VIC as a control assay. The qgPCR reaction mix was prepared using the Prime-
551 Time Gene Expression Master Mix (IDT). Each sample was run in technical triplicates on a
552 LightCycler 480 instrument (Roche). Protocol guidelines were followed to perform the Ct
553 values analysis and total allele number calculation.

Primers	Sequence (5'-3')
MORC2_E27K-gqPCR-F	AGTTGGGGAGCTCTGGAAAG
MORC2_E27K-gqPCR-F	AGGGAAGTGGTTTTGGAGGT
MORC2_E27K-FAM-probe	56-FAM/TTGTTTGGT/ZEN/GCCCTTGCT
MORC2_S87L-gqPCR-F	ACCCTGGGAAAGAAATGCAAA
MORC2_S87L -gqPCR-F	GCTACTCGAGAAACCACCACT
MORC2_ S87L -FAM-probe	56-FAM/TGGGCAGTA/ZEN/CGGGAATGG

554 **Table 4. Primers for quantitative genotyping qPCR.**
555
556 **Bulk RNA sequencing and analysis.**
557 RNA was extracted from cells and organoids using the RNeasy mini and QIAshredder kits
558 (Qiagen) respectively. Sequencing libraries were prepared using the Illumina TruSeq Stranded
559 mRNA Library prep kit optimized for long fragments and subsequently sequenced on a
560 NovoSeq X Plus platform with paired end reads (2x150bp) sequencing.
561 *Genes and repetitive element subfamilies quantification.* The generated reads were mapped
562 to the human reference genome hg38 (GRCh38) with STAR aligner (v 2.6.0)[68] with modified
563 parameters (--outFilterMultimapNmax 100 and --winAnchorMultimapNmax 200). BAM files

564 were sorted using SAMtools (v 1.16.1).[69] For visualisation, BigWig files were created from the
565 BAM files using bamCoverage (v 2.5.4) applying RPKM normalization. Gene quantification was
566 conducted with Subread featureCounts (v1.6.3; flags -p and -s 2 for paired-end reads and
567 strand-specific reads, respectively) using the reference annotation GENCODE version 38.
568 Repetitive elements quantification at a subfamily level was conducted with TEtranscripts (v
569 2.2.3) using default options and using a curated annotation file.[70]
570 *Individual repetitive elements quantification.* To obtain an accurate quantification of
571 individual repetitive elements, alignment of the reads to the reference genome with STAR
572 aligner was conducted to allow only for uniquely mapped reads. To this end, the reads were
573 allowed to map only to a single locus (--outFilterMultimapNmax 1) and the allowed
574 mismatched ratio was decreased (--outFilterMismatchNoverLmax 0.03) compared to default
575 settings. After sorting the obtained BAM files with SAMtools, the quantification was
576 conducted with featureCounts (v1.6.3) using the curated annotation file provided within the
577 TEtranscripts package. Generation of the BigWig files was conducted as described above.
578 *Differential expression analysis.* Differential expression analysis was conducted with DESeq2
579 (v 1.40.2)[71] using as input the count matrices obtained from featureCounts and TEtranscripts.
580 Raw reads were normalized with DESeq2's median-of-ratios normalization method and fold
581 changes were shrunk using DESeq2's lfcShrink. For creating the heatmaps, the mean of
582 replicates for each condition + 0.5 was used and further visualized with pheatmap.
583
584 **Nuclear isolation**.
585 Nuclei extraction was performed from day-15 organoids according to previously described
586 protocols.[72,73] Briefly, organoids were dissociated in cold lysis buffer (0.32 M sucrose, 5 mM
587 $CaCl_2$, 3 mM MgAc, 0.1 mM Na_2EDTA, 10 mM Tris-HCl, pH 8.0, 1 mM DTT) using a 1ml tissue
588 douncer (Wheaton). Isolation was sucrose gradient-based, thus the lysate was layered
589 carefully on top of a sucrose cusion (1.8 M sucrose, 3 mM MgAc, 10 mM Tris-HCl pH 8.0, and
590 1 mM DTT diluted in milliQ water) and then centrifuged for 2h and 15 minutes at 30,000xg 4
591 ^{o}C. Supernatant was thoroughly aspirated, pellet was soften for 10 minutes by adding nuclear
592 storage buffer (15% sucrose, 10 mM Tris-HCl pH 7.2, 70 mM KCl, and 2 mM $MgCl_2$, all diluted
593 in milliQ water), resuspended in dilution buffer (10 mM Tris-HCl pH 7.2, 70 mM KCl, and 2 mM
594 $MgCl_2$, diluted in milliQ water) and filtered using a 70um cell strainer. Finally, nuclei were
595 sorted using FACS (Aria, BD Biosciences) at low flow rate and 4° C.

596

597 **Single-nuclei RNA-sequencing and analysis.**

598 Approximately 8,500 to 10,000 nuclei per sample were prepared for single-nucleus RNA
599 sequencing and loaded onto the Chromium Next GEM Chip G using the Single Cell Kit, along
600 with the reverse transcription mastermix, following the manufacturer's protocol for the
601 Chromium Next GEM Single Cell 3' Kit (10X Genomics, PN-1000268). Single-cell gel beads in
602 emulsion (GEMs) were generated during this process. cDNA was then amplified according to
603 guidelines from 10X Genomics, using 13 PCR cycles for the 3' libraries. Sequencing libraries
604 were constructed with unique dual indices (TT set A), pooled, and sequenced on a NovaSeq X
605 Plus system using a 100-cycle kit with 28-10-10-90 read lengths. Cell Ranger count (v 6.0.0)
606 was run with default settings,[74] with an mRNA and pre-mRNA reference for single-cell samples
607 (generated using 10x Genomics Cell Ranger 6.0.0 guidelines) for single-nucleus samples.
608 Samples clustering was analyzed using Seurat (version 5.1.0).[75] Each sample was filtered
609 according to two criteria, I) nuclei with percentage of mitochondrial content over 2%
610 (perc_mitochondrial) and II) nuclei with number of features (n_Feature) lower than 600 and
611 greater than 2 standard deviations were filtered out. The counts were normalized using
612 Seurat's LogNormalize (NormalizeData) and clusters were defined with a resolution of 0.1
613 (FindClusters). Standard Seurat functions (e.g. DimPlot and DotPlot) were used for all
614 downstream visualization of the data.

615

616 **Oxford Nanopore sequencing and analysis.**

617 For each sample, high molecular weight DNA was extracted from pooled organoids (n = 3)
618 using the Nanobind HMW DNA extraction kit (PacBio) according to manufacturer´s
619 instructions. Extracted DNA was then depleted of short DNA fragments (< 10 kb) and sheared
620 to 10 kb using the Short Reads Eliminator (SRE) XS kit (PacBio) and the g-TUBE (Covaris),
621 respectively. The sequencing libraries for LacZ control and MORC2 CRISPRi samples were
622 prepared using the Ligation Sequencing Kit V14 (SQK-LSK114 - ONT), while for the WT control
623 (clones P14 and 14.3) and S87L MORC2 mutant (clones 87.18 and 87.22) the library was
624 prepared, and the clones were barcoded and using the Native Barcoding Kit 24 V14 (SQK-
625 NBD114.24 - ONT). All libraries were sequenced on FLO-PRO114M flow cells on a PromethION
626 device (ONT) for 72 h. Basecalling and alignment to the human reference genome hg38 was
627 conducted with Dorado (v0.7.1) using the DNA model dna_r10.4.1_e8.2_400bps_sup@v4.3.0

628 and the DNA modification model dna_r10.4.1_e8.2_400bps_sup@v4.3.0_5mCG_5hmCG@v1
629 for the detection of CpG methylation. Resulting BAM files were sorted with SAMtools (v1.18).
630 Methylartist (v1.3.0) was used for the subsequent analysis of the methylation data visualised
631 through Methylartist and R (v4.4.2).[76] Modkit (v0.3.3) and BedGraphToBigWig (v4) were used
632 to produce bedGraph from the BAM files and BigWigs from the bedGraph files, respectively.
633 The BigWig files were then used for visualisation of the methylation with computeMatrix and
634 plotHeatmap (DeepTools v2.5.4).
635
636 **CUT&RUN.**
637 Two different CUT&RUN approaches were followed. For profiling histone modifications
638 (H3K4me3, H3K9me3, H3K27Ac), a standard CUT&RUN protocol was used. To profile MORC2
639 chromatin binding, a crosslinked protocol was used.
640 *Standard CUT&RUN.* The CUT&RUN protocol used here has previously been described.[77,78]
641 Briefly, 500k cells were harvested as described above (see cell culture: hiPSCs or SHSY5Y) and
642 washed three times using Wash buffer containing 20 mM HEPES pH 7.5, 150 mM NaCl, 0.5
643 mM spermidine, 1x Roche cOmplete protease inhibitors. Cells were then incubated and
644 attached to 10 uL pre-activated ConA-coated magnetic beads (Bangs Laboratories) on an end-
645 to-end rotator for 7-10 min. To activate ConA-coated magnetic beads, they were washed
646 twice with binding buffer containing 20 mM HEPES pH 7.9, 10 mM KCl, 1 mM $CaCl_2$, 1 mM
647 $MnCl_2$. Bead-bound cells then were incubated with primary antibody solution (20 mM HEPES
648 pH 7.5, 0.15 M NaCl, 0.5 mM Spermidine, 1x Roche complete protease inhibitors, 0.05% w/v
649 digitonin, 2 mM EDTA and 1:100 primary antibody) overnight at 4 ^{o}C. On the second day,
650 bead-bound cells were washed twice using digitonin buffer (20 mM HEPES pH 7.5, 150 mM
651 NaCl, 0.5 mM Spermidine, 1x Roche cOmplete protease inhibitors, 0.05% digitonin) then
652 incubated with pAG-MNase enzyme resuspended in digitonin buffer at 4 ^{o}C for 1 h with a
653 gentle mixing. Bead-bound cells were then washed twice with digitonin buffer, resuspended
654 in 100μL digitonin buffer, chilled to 0 ^{o}C for 5 min then incubated for 30 min at 0 ^{o}C with 2 mM
655 CaCl2 to activate genome cleavage. Finally, the reaction was quenched by adding 100 mL 2x
656 stop buffer (0.35 M NaCl, 20 mM EDTA, 4mM EGTA, 0.05% digitonin, 50 ng/mL glycogen, 50
657 ng/mL RNase A) and gentle vortexing followed by a 30 min incubation at 37 ^{o}C to release the
658 genomic fragments. The supernatant was collected and purified using PCR clean-up spin
659 columns (Macherey-Nagel).

660 *Day-15 organoid CUT&RUN.* 3-6 organoids per cell line was used. Organoids were collected
661 on day-15 of differentiation, washed with PBS, and incubated 3 minutes with Accutase on a
662 shaker at 37 °C to dissociate cells. They were then gently resuspended in Accutase and
663 incubated on the shaker for another 4 minutes followed by a 5-minute centrifugation at 400xg.
664 Finally, the cell suspension was filtered to remove Matrigel. The standard *CUT&RUN* protocol
665 was followed as described above.
666 *Crosslinked CUT&RUN.* The approach was same as above with addition of the followings: a
667 cross-linking step, an increase in cell number and a slightly higher centrifugation force. 900K-
668 1M cells were collected by centrifugation at 600xg for 3 minutes and crosslinked for 1 min
669 using 1% formaldehyde (in cell culture media, diluted from a 16% solution, Thermo Scientific).
670 Cross-linked cells were then washed three times with wash buffer containing 20 mM HEPES
671 pH 7.5, 150 mM NaCl, 0.5 mM spermidine, 1x Roche complete protease inhibitors, 1% Triton
672 X-100, 0.05% SDS. To avoid loss of the crosslinked cell/nuclear pellet during washes, a slight
673 increase in centrifugation speed (1000-1300xg) was applied. Cells were incubated with ConA
674 beads for 7-10 minutes as above and then resuspended in primary antibody buffer (20 mM
675 HEPES pH 7.5, 150 mM NaCl, 0.5 mM spermidine, 1x Roche complete protease inhibitors, 1%
676 Triton X-100, 0.05% SDS, 0.05% digitonin, 2 mM EDTA). After an overnight incubation at 4 °C
677 with the primary antibody, bead-bound cells were thoroughly washed two times with
678 digitonin buffer (20 mM HEPES pH 7.5, 150 mM NaCl, 0.5 mM Spermidine, 1x Roche complete
679 protease inhibitors, 1% Triton X-100, 0.05% SDS, 0.05% digitonin). Following the 37 °C
680 incubation to release genomic fragments, 0.09% SDS and 0.22 mg/ml proteinase K (Thermo
681 Scientific) was added to supernatant to reverse the crosslinking reaction. Finally, DNA was
682 purified using PCR clean-up spin column (Macherey-Nagel).
683
684 **CUT&RUN sequencing and analysis.**
685 Hyperprep kit (KAPA) with unique dual indexed adaptors were used to prepare sequencing
686 libraries which were then pooled and sequenced on NovaSeqX plus machine
687 (Illumina). Paired-end reads (2×75) were aligned to the human genome (GRCh38) using
688 bowtie2 (v 2.4.5) (–local –very-sensitive-local –no-mixed –no-unal –no-discordant –phred33
689 -I 10 -X 700),[79] converted to BAM files and further sorted with SAMtools (v 1.16.1). Reads per
690 kilobase per million mapped reads (RPKM)-normalized BigWig coverage tracks were made
691 with bamCoverage (DeepTools, v 2.5.4). Heatmaps matrices were created by computeMatrix

692 (DeepTools v2.5.4) using called peaks as the input regions and RPKM normalized bigwigs as
693 input signal. Matrices were then visualized using plotHeatmap (DeepTools, v2.5.4), adjusting
694 the upstream and downstream visualization parameters (-a and -b) and splitting the signal in
695 heatmaps (--kmeans 2).
696
697 **Immunostaining**.
698 *hiPSCs immunostaining.* Cells cultured on 24-well ibidi plates were rinsed three times with
699 DPBS and fixed in 4% formaldehyde for 15 min at room temperature. Before blocking with
700 TKPBS (KPBS with 0.25% Triton X-100) and 5% Normal Donkey Serum (NDS), cells were
701 washed another three times with DPBS. After 1h blocking, they were incubated overnight at
702 4 °C with primary antibody or TKPBS + 5% NDS for negative controls. The next day cells were
703 rinsed in TKPBS twice for 5 minutes each and once in TKBPS/ 5% NDS. They were then
704 incubated with secondary antibody solution (TKPBS + 5% NDS) at room temperature for 2 h
705 followed by a 5-minute incubation with DAPI (1:1000, Sigma D817) diluted in TKPBS. After
706 two washes with KPBS, cells were imaged using a Zeiss 780 confocal microscope.
707 *Day-15 organoid immunostaining.* Organoids harvested at day 15 of differentiation were
708 gently rinsed once with DPBS (Gibco) in 24-well plates then fixed with 4% paraformaldehyde
709 (PFA) for 90-120 minutes at room temperature. After fixation, organoids were washed three
710 times with KPBS for 10 minutes each time and incubated overnight with 30% sucrose at 4 °C
711 overnight on gentle shake. The following day, organoids were immersed in OCT (catalog no.
712 45830, HistoLab), snap frozen on dry ice and stored in -20°C until use. Before staining,
713 organoids were sliced into 20-μm sections using a cryostat (Thermo Scientific Cryostar NX70)
714 at -20°C and placed onto Superfrost Plus microscope slides. Borders of each slide were
715 defined using a hydrophobic PAP Pen before starting the immunostaining. After two washes
716 with KPBS, slides were incubated with blocking solution (TKPBS & 5% NDS) for 1 h at room
717 temperature. They were then incubated with primary antibody solution (relevant primary
718 antibody diluted in TKPBS & 5% NDS) overnight at 4 °C. The following day slides were washed
719 three times with KPBS and incubated with secondary antibody solution for 1 h at room
720 temperature. Finally, after three more washes, slides were incubated with DAPI, rinsed off
721 with KPBS, mounted using FluorSave mounting medium and imaged with a Zeiss 780 Confocal
722 microscope. Further image adjustments were performed in batch on Image J.
723

724 **STORM.**

725 Cells were seeded on glass 8-well Ibidi dishes and next day fixed with 4% formaldehyde in PBS
726 for 15 min. Membranes were permeabilised with 0.1% Triton-X100 in PBS for 5 min. For
727 staining, wells were first blocked with 10% FBS in PBS then incubated with primary anti-HA
728 antibody at 1/500 followed by secondary Alexa Fluor 647 at 1/1000. After washing samples
729 were fixed again for 5 min, washed and kept in PBS at 4°C till the imaging. STORM data was
730 acquired using Nikon N-STORM inverted microscope with 647 nm laser line, Apochromat TIRF
731 100×/1.49 NA oil immersion objective and single-photon detection iXon Ultra DU897 EMCCD
732 camera (Andor). Samples were washed with PBS and then STORM buffer (7mM NaOH, 100
733 mM mercaptoethylamine (MEA) in PBS) was added for the imaging. Samples were illuminated
734 with the 647 nm laser at 2–3 $kW \cdot cm^{-2}$ and 100 000 frames were collected for each field of
735 view at a frame rate of 50–70 Hz. Data was processed in NIS elements Advanced Research
736 with N-STORM module. Further image processing and cropping was performed using ImageJ.
737

738 **Western blot.**

739 Cell lysis was performed using either RIPA (Sigma-Aldrich) containing complete protease
740 inhibitor cocktail or 1:100 benzonase in 1% SDS on ice for 30 minutes and pelleted for 20
741 minutes at 4 °C and 12,000x*g*. Before running on a 4–12% Tris-glycine SDS-PAGE gel (200 V,
742 40-45 min, RT) (Life Technologies), supernatant was aspirated into new tubes and mixed with
743 loading dye (Novex LDS 4x) and reducing agent (Thermo) then boiled for 10 minutes at 70 °C.
744 To transfer proteins from gel to membrane, pre-made transfer stacks were used (Transblot-
745 Turbo Transfer system, BioRad) according to manufacturer's instructions. Membrane was
746 briefly rinsed with TBS-T (Tris-buffered saline with 0.1% Tween) and blocked in 5% skimmed
747 milk diluted in TBS-T (MTBST) for 1h at RT on a shaker. Membrane was rinsed once in TBS-T
748 and incubated at 4 °C overnight (for abundant targets e.g., Actin 1h incubation at RT is
749 sufficient) with primary antibody diluted in MTBST. The following day membrane was washed
750 three times in TBS-T each time for 5-10 minutes with shaking. It was then incubated with HRP-
751 conjugated anti-mouse (Cell signalling) or anti-rabbit secondary antibody (Santa Cruz
752 Biotechnology, 1:5,000) diluted in MTBST. Before protein detection, membrane was washed
753 three times in TBS-T each time for 5-10 minutes with shaking and once with TBS. Protein was
754 detected by chemiluminescence using ECL Select reagents (Cytiva) according to
755 manufacturer's instructions and imaged on a Chemi-Doc system (BioRad). Finally, β-actin

staining was performed by stripping the membrane using the Restore PLUS Western Blot Stripping Buffer (Thermo) as per instructions, and re-blocking for 1 h in MTBST.

Antibodies.

CUT&RUN: Goat anti-rabbit IgG (abcam ab97047), Rabbit anti-H3K4me3 (Active Motif 39159), Rabbit anti-MORC2(A300-149A, Bethyl), Rabbit anti HA-Tag (C29F4) mAb 3724, Rabbit anti-H3K9me3 (abcam 8898), Rabbit anti-H3K27ac (MABE647 clone RM172) (1:50-1:100 dilution).

Immunostaining: Rabbit anti-NANOG (1:600 dilution, Abcam, RRID: AB446437), Mouse anti-OCT3/4 (1:300 dilution,Santa Cruz, RRID: AB628051), Rabbit anti-Sox2 1:500 (Merck AB5603, RRID: AB2286686), DAPI (1:1000 dilution, Sigma-Aldrich), Mouse anti-ORF1p, clone 4H1 (1:300 dilution, Sigma-Aldrich, RRID: RRID:AB2941775), Rabbit anti-PAX6 (1:300, Biolegend, 901301), Mouse anti-ZO1 (1:300, Invitrogen, 339100), Mouse anti-HA11 (Biolegend, 901501) ,Donkey anti-mouse Cy3 (1:500 dilution, Jackson Lab), Donkey anti-rabbit Alexa647 (1:500 dilution,Jackson Lab), Alexa-488 anti-mouse (Thermofisher, A21202, RRID AB141607), Alexa-568 anti-rabbit (Thermofisher A10042, RRID AB2534017).

Western Blot: Rabbit anti-MORC2 (A300-149A, Bethyl), Rabbit mAb HA-Tag (C29F4), Anti LINE-1 ORF1p clone 4H1 (Merck Millipore, MABC1152), HRP-472 conjugated anti-β-actin (1:50000 dilution Sigma A3854), HRP-conjugated anti-mouse IgG (1:10000, Cell signalling 7076P2), HRP-conjugated anti-rabbit IgG (1:5000, Santa Cruz Biotechnology), Mouse α-β-actin (abcam ab8226).

DATA AVAILABILITY.

There are no restrictions on data availability. The RNA and DNA sequencing data presented in this study have been deposited at GEOs: GSEXXXXX.

REFERENCES.

1. Nurk, S. *et al.* The complete sequence of a human genome. *Science (1979)* **376**, (2022).
2. Ewing, A. D. *et al.* Nanopore Sequencing Enables Comprehensive Transposable Element Epigenomic Profiling. *Mol Cell* (2020) doi:10.1016/j.molcel.2020.10.024.
3. Garza, R. *et al.* LINE-1 retrotransposons drive human neuronal transcriptome complexity and functional diversification. *Sci Adv* **9**, (2023).

788 4. Criscione, S. W. *et al.* Genome-wide characterization of human L1 antisense promoter-
789 driven transcripts. *BMC Genomics* **17**, (2016).

790 5. Rangwala, S. H., Zhang, L. & Kazazian, H. H. Many LINE1 elements contribute to the
791 transcriptome of human somatic cells. *Genome Biol* **10**, (2009).

792 6. Beck, C. R. *et al.* LINE-1 retrotransposition activity in human genomes. *Cell* (2010)
793 doi:10.1016/j.cell.2010.05.021.

794 7. Brouha, B. *et al.* Hot L1s account for the bulk of retrotransposition in the human
795 population. *Proc Natl Acad Sci U S A* **100**, (2003).

796 8. Liu, N. *et al.* Selective silencing of euchromatic L1s revealed by genome-wide screens
797 for L1 regulators. *Nature* **553**, 228–232 (2018).

798 9. Ilık, İ. A. *et al.* Autonomous transposons tune their sequences to ensure somatic
799 suppression. *Nature* **626**, (2024).

800 10. Marasca, F. *et al.* LINE1 are spliced in non-canonical transcript variants to regulate T
801 cell quiescence and exhaustion. *Nat Genet* **54**, (2022).

802 11. Attig, J. *et al.* Heteromeric RNP Assembly at LINEs Controls Lineage-Specific RNA
803 Processing. *Cell* (2018) doi:10.1016/j.cell.2018.07.001.

804 12. Greenberg, M. V. C. & Bourc'his, D. The diverse roles of DNA methylation in mammalian
805 development and disease. *Nature Reviews Molecular Cell Biology* vol. 20
806 https://doi.org/10.1038/s41580-019-0159-6 (2019).

807 13. Jönsson, M. E. *et al.* Activation of neuronal genes via LINE-1 elements upon global DNA
808 demethylation in human neural progenitors. *Nat Commun* (2019) doi:10.1038/s41467-
809 019-11150-8.

810 14. Deniz, Ö., Frost, J. M. & Branco, M. R. Regulation of transposable elements by DNA
811 modifications. *Nature Reviews Genetics* vol. 20 https://doi.org/10.1038/s41576-019-
812 0106-6 (2019).

813 15. Walsh, C. P., Chaillet, J. R. & Bestor, T. H. Transcription of IAP endogenous retroviruses
814 is constrained by cytosine methylation [4]. *Nature Genetics* vol. 20
815 https://doi.org/10.1038/2413 (1998).

816 16. Oomen, M. E. *et al.* An atlas of transcription initiation reveals regulatory principles of
817 gene and transposable element expression in early mammalian development. *Cell* **188**,
818 1156-1174.e20 (2025).

819 17. Grow, E. J. *et al.* Intrinsic retroviral reactivation in human preimplantation embryos and
820 pluripotent cells. *Nature* **522**, (2015).

821 18. Jachowicz, J. W. *et al.* LINE-1 activation after fertilization regulates global chromatin
822 accessibility in the early mouse embryo. *Nat Genet* **49**, (2017).

823 19. Macfarlan, T. S. *et al.* Embryonic stem cell potency fluctuates with endogenous
824 retrovirus activity. *Nature* **487**, (2012).

825 20. Percharde, M. *et al.* A LINE1-Nucleolin Partnership Regulates Early Development and
826 ESC Identity. *Cell* (2018) doi:10.1016/j.cell.2018.05.043.

827 21. Ozata, D. M., Gainetdinov, I., Zoch, A., O'Carroll, D. & Zamore, P. D. PIWI-interacting
828 RNAs: small RNAs with big functions. *Nature Reviews Genetics* vol. 20
829 https://doi.org/10.1038/s41576-018-0073-3 (2019).

830 22. Rowe, H. M. *et al.* KAP1 controls endogenous retroviruses in embryonic stem cells.
831 *Nature* (2010) doi:10.1038/nature08674.

832 23. Turelli, P. *et al.* Interplay of TRIM28 and DNA methylation in controlling human
833 endogenous retroelements. *Genome Res* (2014) doi:10.1101/gr.172833.114.

834 24. Imbeault, M., Helleboid, P. Y. & Trono, D. KRAB zinc-finger proteins contribute to the
835 evolution of gene regulatory networks. *Nature* (2017) doi:10.1038/nature21683.

836 25. de Tribolet-Hardy, J. *et al.* Genetic features and genomic targets of human KRAB-zinc
837 finger proteins. *Genome Res* **33**, (2023).

838 26. Jacobs, F. M. J. *et al.* An evolutionary arms race between KRAB zinc-finger genes
839 ZNF91/93 and SVA/L1 retrotransposons. *Nature* (2014) doi:10.1038/nature13760.

840 27. Smith, Z. D. *et al.* DNA methylation dynamics of the human preimplantation embryo.
841 *Nature* **511**, (2014).

842 28. Adami, A. *et al.* LINE-1 retrotransposons regulate the exit of human pluripotency and
843 early brain development. *bioRxiv* 2025.01.17.633315 (2025)
844 doi:10.1101/2025.01.17.633315.

845 29. Klawitter, S. *et al.* Reprogramming triggers endogenous L1 and Alu retrotransposition
846 in human induced pluripotent stem cells. *Nat Commun* **7**, (2016).

847 30. Lanciano, S. *et al.* Locus-level L1 DNA methylation profiling reveals the epigenetic and
848 transcriptional interplay between L1s and their integration sites. *Cell Genomics* **4**,
849 (2024).

850 31. Sanchez-Luque, F. J. *et al.* LINE-1 Evasion of Epigenetic Repression in Humans. *Mol Cell*
851 (2019) doi:10.1016/j.molcel.2019.05.024.

852 32. Tchasovnikarova, I. A. *et al.* Hyperactivation of HUSH complex function by Charcot-
853 Marie-Tooth disease mutation in MORC2. *Nat Genet* **49**, 1035–1044 (2017).

854 33. Pandiloski, N. *et al.* DNA methylation governs the sensitivity of repeats to restriction by
855 the HUSH-MORC2 corepressor. *Nat Commun* **15**, 7534 (2024).

856 34. Hagelkruys, A. *et al.* The HUSH complex controls brain architecture and protocadherin
857 fidelity. *Sci Adv* **8**, (2022).

858 35. Robbez-Masson, L. *et al.* The hush complex cooperates with trim28 to repress young
859 retrotransposons and new genes. *Genome Res* (2018) doi:10.1101/gr.228171.117.

860 36. Fendler, N. L. *et al.* Identification and characterization of a human MORC2 DNA binding
861 region that is required for gene silencing. *Nucleic Acids Res* **53**, gkae1273 (2025).

862 37. Douse, C. H. *et al.* Neuropathic MORC2 mutations perturb GHKL ATPase dimerization
863 dynamics and epigenetic silencing by multiple structural mechanisms. *Nat Commun*
864 (2018) doi:10.1038/s41467-018-03045-x.

865 38. Xie, H. Y., Zhang, T. M., Hu, S. Y., Shao, Z. M. & Li, D. Q. Dimerization of MORC2 through
866 its C-terminal coiled-coil domain enhances chromatin dynamics and promotes DNA
867 repair. *Cell Communication and Signaling* **17**, (2019).

868 39. Kim, H. J. *et al.* The Gene-Silencing Protein MORC-1 Topologically Entraps DNA and
869 Forms Multimeric Assemblies to Cause DNA Compaction. *Mol Cell* (2019)
870 doi:10.1016/j.molcel.2019.07.032.

871 40. Harris, C. J. *et al.* Arabidopsis AtMORC4 and AtMORC7 Form Nuclear Bodies and
872 Repress a Large Number of Protein-Coding Genes. *PLoS Genet* **12**, (2016).

873 41. Weiser, N. E. *et al.* MORC-1 Integrates Nuclear RNAi and Transgenerational Chromatin
874 Architecture to Promote Germline Immortality. *Dev Cell* **41**, 408–423 (2017).

875 42. Moissiard, G. *et al.* MORC family ATPases required for heterochromatin condensation
876 and gene silencing. *Science* **336**, 1448–51 (2012).

877 43. Iyer, L. M., Abhiman, S. & Aravind, L. MutL homologs in restriction-modification
878 systems and the origin of eukaryotic MORC ATPases. *Biol Direct* **3**, 8 (2008).

879 44. Chen, S. *et al.* A genomic mutational constraint map using variation in 76,156 human
880 genomes. *Nature* **625**, (2024).

881 45. Sevilla, T. *et al.* Mutations in the MORC2 gene cause axonal Charcot-Marie-Tooth
882 disease. *Brain* **139**, 62–72 (2016).

883 46. Guillen Sacoto, M. J. *et al.* De Novo Variants in the ATPase Module of MORC2 Cause a
884 Neurodevelopmental Disorder with Growth Retardation and Variable Craniofacial
885 Dysmorphism. *Am J Hum Genet* (2020) doi:10.1016/j.ajhg.2020.06.013.

886 47. Peymani, F. *et al.* Pleiotropic effects of MORC2 derive from its epigenetic signature.
887 *Brain* awaf159 (2025) doi:10.1093/brain/awaf159.

888 48. Tailor, J. *et al.* Stem cells expanded from the human embryonic hindbrain stably retain
889 regional specification and high neurogenic potency. *Journal of Neuroscience* **33**, (2013).

890 49. Hanley, J. G., Koulen, P., Bedford, F., Gordon-Weeks, P. R. & Moss, S. J. The protein
891 MAP-1B links GABAC receptors to the cytoskeleton at retinal synapses. *Nature* **397**, 66–
892 69 (1999).

893 50. Grassi, D. A. *et al.* Profiling of lincRNAs in human pluripotent stem cell derived forebrain
894 neural progenitor cells. *Heliyon* (2020) doi:10.1016/j.heliyon.2019.e03067.

895 51. Seczynska, M., Bloor, S., Cuesta, S. M. & Lehner, P. J. Genome surveillance by HUSH-
896 mediated silencing of intronless mobile elements. *Nature* (2022) doi:10.1038/s41586-
897 021-04228-1.

898 52. Douse, C. H. *et al.* TASOR is a pseudo-PARP that directs HUSH complex assembly and
899 epigenetic transposon control. *Nat Commun* (2020) doi:10.1038/s41467-020-18761-6.

900 53. Li, X. *et al.* A Maternal-Zygotic Effect Gene, Zfp57, Maintains Both Maternal and
901 Paternal Imprints. *Dev Cell* **15**, (2008).

902 54. Takahashi, N. *et al.* ZNF445 is a primary regulator of genomic imprinting. *Genes Dev* **33**,
903 (2019).

904 55. Petropoulos, S. *et al.* Single-Cell RNA-Seq Reveals Lineage and X Chromosome
905 Dynamics in Human Preimplantation Embryos. *Cell* **165**, (2016).

906 56. Kagawa, H. *et al.* Human blastoids model blastocyst development and implantation.
907 *Nature* **601**, (2022).

908 57. Janssen, S. M. & Lorincz, M. C. Interplay between chromatin marks in development and
909 disease. *Nature Reviews Genetics* vol. 23 https://doi.org/10.1038/s41576-021-00416-
910 x (2022).

911 58. Ren, W. *et al.* Direct readout of heterochromatic H3K9me3 regulates DNMT1-mediated
912 maintenance DNA methylation. *Proc Natl Acad Sci U S A* **117**, (2020).

913 59. Pastor, W. A. *et al.* MORC1 represses transposable elements in the mouse male
914 germline. *Nat Commun* **5**, (2014).

915 60. Uneme, Y. *et al.* Morc1 reestablishes H3K9me3 heterochromatin on piRNA-targeted
916 transposons in gonocytes. *Proceedings of the National Academy of Sciences* **121**,
917 e2317095121 (2024).

918 61. Athanikar, J. N., Badge, R. M. & Moran, J. V. A YY1-binding site is required for accurate
919 human LINE-1 transcription initiation. *Nucleic Acids Res* **32**, (2004).

920 62. Uhlin, E. *et al.* Derivation of human iPS cell lines from monozygotic twins in defined and
921 xeno free conditions. *Stem Cell Res* **18**, (2017).

922 63. Nolbrant, S., Heuer, A., Parmar, M. & Kirkeby, A. Generation of high-purity human
923 ventral midbrain dopaminergic progenitors for in vitro maturation and intracerebral
924 transplantation. *Nat Protoc* (2017) doi:10.1038/nprot.2017.078.

925 64. Lancaster, M. A. & Knoblich, J. A. Generation of cerebral organoids from human
926 pluripotent stem cells. *Nat Protoc* **9**, (2014).

927 65. Zufferey, R., Nagy, D., Mandel, R. J., Naldini, L. & Trono, D. Multiply attenuated lentiviral
928 vector achieves efficient gene delivery in vivo. *Nat Biotechnol* (1997)
929 doi:10.1038/nbt0997-871.

930 66. Johansson, P. A., Adami, A. & Jakobsson, J. CRISPRi-mediated transcriptional silencing
931 in iPSCs for the study of human brain development. *STAR Protoc* **3**, (2022).

932 67. Weisheit, I. *et al.* Simple and reliable detection of CRISPR-induced on-target effects by
933 qgPCR and SNP genotyping. *Nat Protoc* **16**, (2021).

934 68. Dobin, A. *et al.* STAR: Ultrafast universal RNA-seq aligner. *Bioinformatics* (2013)
935 doi:10.1093/bioinformatics/bts635.

936 69. Li, H. *et al.* The Sequence Alignment/Map format and SAMtools. *Bioinformatics* (2009)
937 doi:10.1093/bioinformatics/btp352.

938 70. Jin, Y., Tam, O. H., Paniagua, E. & Hammell, M. TEtranscripts: A package for including
939 transposable elements in differential expression analysis of RNA-seq datasets.
940 *Bioinformatics* (2015) doi:10.1093/bioinformatics/btv422.

941 71. Love, M. I., Anders, S. & Huber, W. *Differential Analysis of Count Data - the DESeq2*
942 *Package*. *Genome Biology* (2014). doi:110.1186/s13059-014-0550-8.

943 72. Södersten, E. *et al.* A comprehensive map coupling histone modifications with gene
944 regulation in adult dopaminergic and serotonergic neurons. *Nat Commun* **9**, (2018).

945 73. Jönsson, M. E. *et al.* Activation of endogenous retroviruses during brain development
946 causes an inflammatory response. *EMBO J* (2021) doi:10.15252/embj.2020106423.

947 74. Zheng, G. X. Y. *et al.* Massively parallel digital transcriptional profiling of single cells.
948 *Nat Commun* **8**, (2017).

949 75. Stuart, T. *et al.* Comprehensive Integration of Single-Cell Data. *Cell* **177**, (2019).

950 76. Cheetham, S. W., Kindlova, M. & Ewing, A. D. Methylartist: tools for visualizing modified
951 bases from nanopore sequence data. *Bioinformatics* **38**, (2022).

952 77. Skene, P. J., Henikoff, J. G. & Henikoff, S. Targeted in situ genome-wide profiling with
953 high efficiency for low cell numbers. *Nat Protoc* (2018) doi:10.1038/nprot.2018.015.

954 78. Meers, M. P., Bryson, T. D., Henikoff, J. G. & Henikoff, S. Improved cut&run chromatin
955 profiling tools. *Elife* **8**, (2019).

956 79. Langmead, B. & Salzberg, S. L. Fast gapped-read alignment with Bowtie 2. *Nat Methods*
957 (2012) doi:10.1038/nmeth.1923.

958

959 **ACKNOWLEDGEMENTS.**

960 We thank A. Hammarberg, S. da Rocha Baez, E. Monni, M. Persson-Vejgården, J. Nelander and
961 S. Tesson for their technical assistance, S. Henikoff for the gift of the pA-MNase protein used
962 in initial hNPC CUT&RUN experiments and the pAG-MNase plasmid (Addgene #123461) for in
963 house production of the pAG-MNase used in all subsequent experiments. We thank P. Lehner
964 for providing lentiviral vectors to knockout MORC2 and re-express MORC2 variants, the SCC
965 Cell and Gene Therapy Core at Lund University and iPSC core at Karolinska Institute for
966 generation of MORC2 edited iPSC clones. We acknowledge Clinical Genomics Lund and the
967 Center for Translational Genomics (CTG) at Lund University for providing expertise and service
968 with sequencing and analysis. This work was supported by the Swedish Government Initiative
969 for Strategic Research Areas (MultiPark & StemTherapy) and grants from the Swedish
970 Research Council (VR, 2022-02673 to J.J., 2021-03494 to C.H.D.), the Swedish Brain
971 Foundation (Hjärnfonden, FO2023-0232, FO2023-0229 to C.H.D.), the Swedish Society for
972 Medical Research (SSMF, S19-0100 to C.H.D.), Cancerfonden (222185Pj to J.J.),
973 Barncancerfonden (PR2023-0099 to J.J.) and the Wellcome Trust (101908/Z/13/Z and
974 217191/Z/19/Z to Y.M.). This project has been made possible in part by grant 2023-331773 to
975 C.H.D. from the Chan Zuckerberg Initiative DAF, an advised fund of the Silicon Valley
976 Community Foundation. Finally, we also acknowledge The Royal Physiographic Society of
977 Lund (project grant to F.D.), the Crafoord Foundation and Bente-Rexed-Gerstedt Foundation
978 (project grants to C.H.D.).

979 **AUTHOR CONTRIBUTIONS.**

980 AA made and validated the SHSY5Y MORC2 KO cell line and complemented cell lines. FD and
981 LC-V designed and performed iPSC culture and cerebral organoid differentiations. FD, SK, SB
982 and AK performed CUT&RUN experiments. FD, LC-V and CD-H performed quality control
983 analysis of iPSC lines. CF prepared DNA for Nanopore sequencing and performed
984 bioinformatic analysis of the data. CF, NP and SK processed Illumina sequencing experiments
985 and performed bioinformatic analysis of the data. JM, OEK and CD-H tested neural
986 differentiation protocols. FD, LC-V and AAd performed nuclear isolation. JGJ prepared all

Illumina sequencing libraries for bulk and single-nuclei RNA-seq and CUT&RUN experiments. CHD conceived and designed the study. YM, JJ and CHD supervised the study and acquired funding. FD, CF and CHD wrote the manuscript and made figures with assistance from NP. All authors reviewed the final version.

1011 **SUPPLEMENTARY FIGURES.**

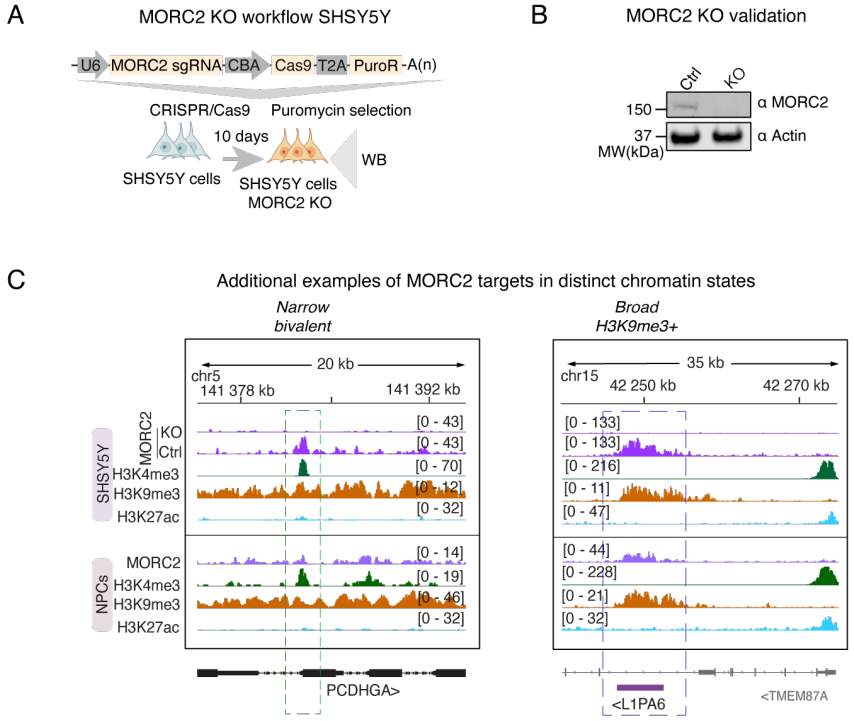

1012

1013 **Supplementary Figure 1. (A)** Workflow for generating the MORC2 KO SHSY5Y cell line. **(B)** Validation of MORC2
1014 KO by Western blot. **(C)** Further examples of the different chromatin states characterizing MORC2 targets, see
1015 also Fig 1.

1016

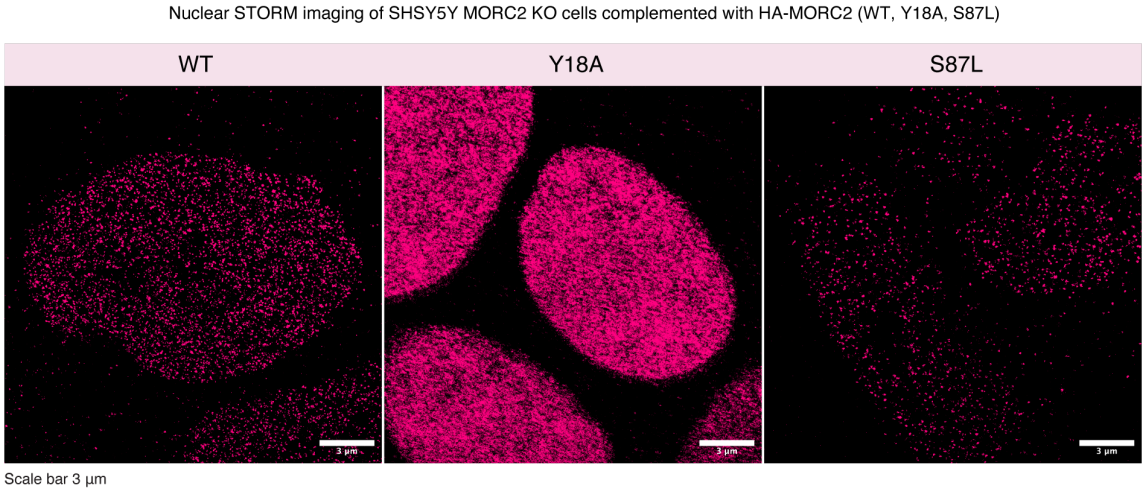

1017

1018 **Supplementary Figure 2.** Nuclear STORM imaging of SHSY5Y MORC2 KO cells complemented with HA-MORC2
1019 (WT, Y18A, S87L) targeting the HA epitope tag.

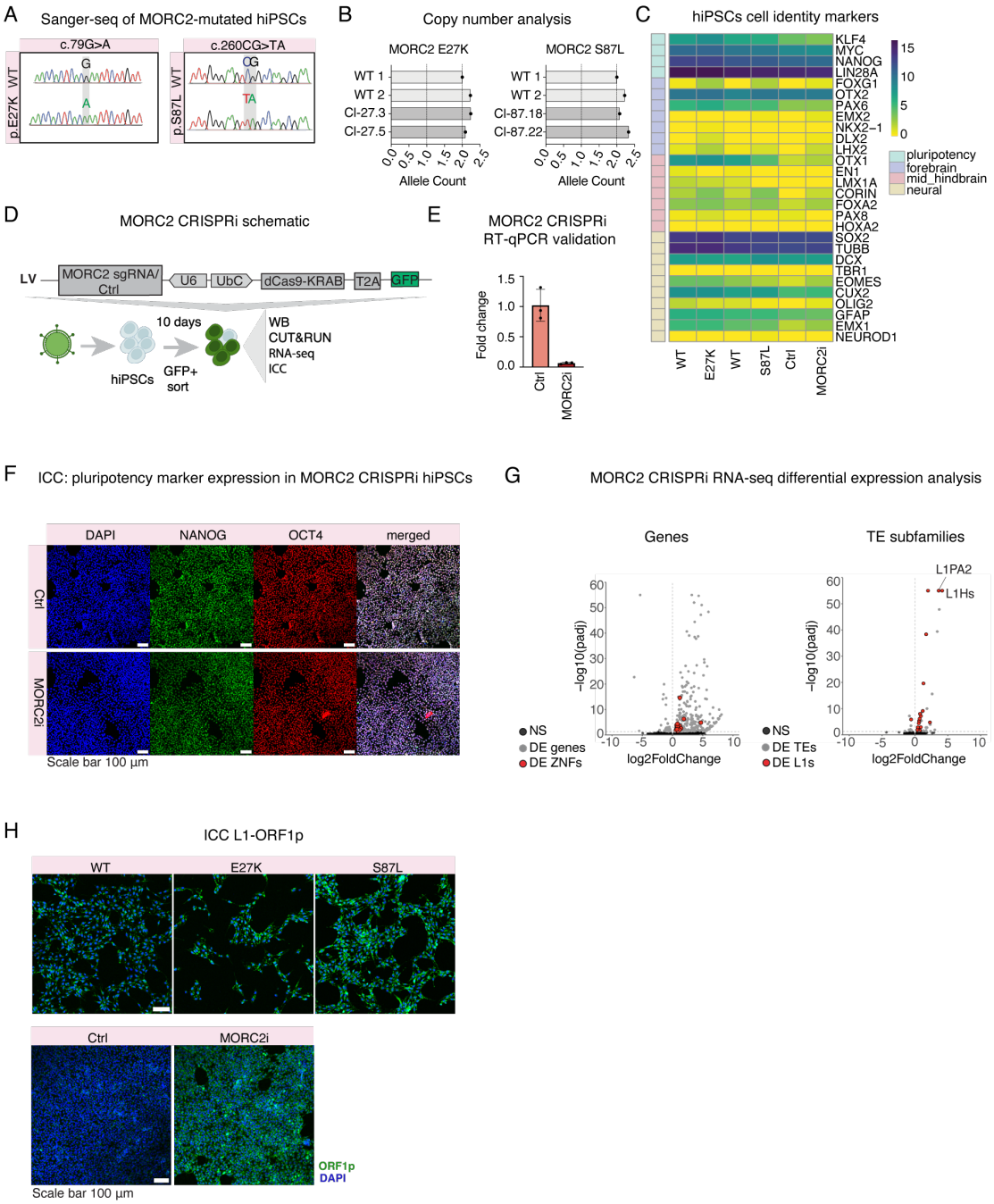

Supplementary Figure 3. (A) Electropherogram of the Sanger sequencing confirming the CRISPR-directed MORC2 mutations (E27K and S87L) in representative clones **(B)** Copy number analysis showing allele count for each MORC2 mutant clone and WT hiPSC lines. **(C)** Unscaled heatmap showing normalized read counts of pluripotency and neural marker genes as calculated by DESeq2 in the hiPSCs used in the study. Two batches of RNA from each clone was used for WT (n=4), E27K (n=4) and S87L (n=4) genotypes. **(D)** Schematic workflow of MORC2 CRISPRi experiment in hiPSCs and subsequent analyses. **(E)** Validation of CRISPRi through RT-qPCR analysis of MORC2 expression in control (n=3) and CRISPRi (n=3) hiPSCs. **(F)** Immunohistochemistry of pluripotency markers (NANOG, OCT4) for MORC2 control and CRISPRi cell lines. **(G)** Volcano plot showing the results of the differential expression analysis (DESeq2) for genes (left) and TE subfamilies using TEtranscripts (right) in the MORC2 CRISPRi cell line (n=3) compared to control (n=3). Differentially expressed genes and LINE1 subfamilies are highlighted in red, other differentially expressed genes and subfamilies are presented in grey (padj <0.05). **(H)** Immunohistochemistry of L1-ORF1p (green) in E27K and S87L MORC2 mutant and CRISPRi cell lines with their respective controls. Experiments were performed at least twice with similar results.

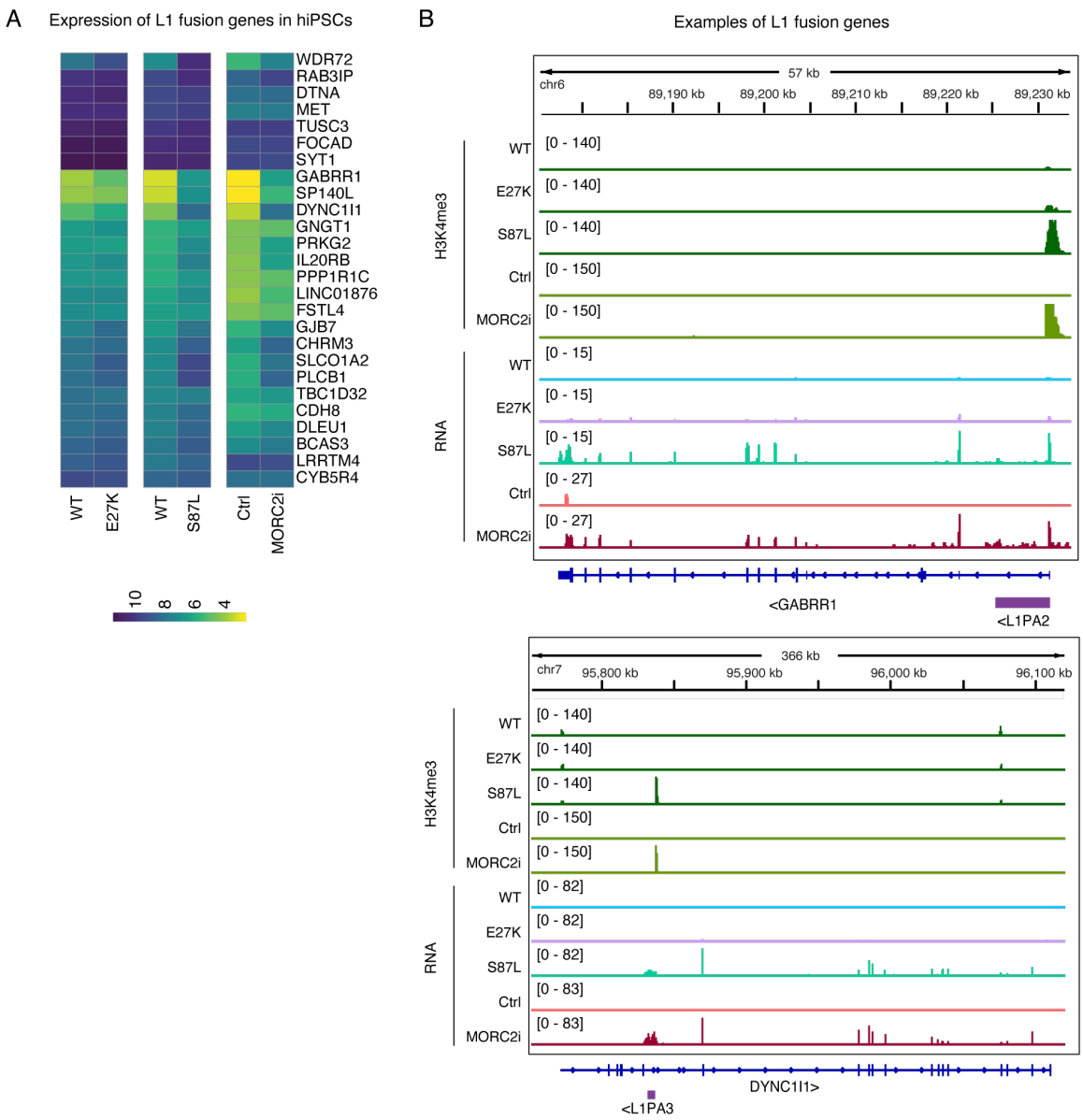

Supplementary Figure 4. (A) Unscaled heatmap showing the normalized read counts of L1 fusion genes in the E27K (n=4) and S87L (n=4) MORC2 mutant iPSC lines as compared to WT controls (n=4) and MORC2 CRISPRi (n=3) iPSCs compared to its control (n=3). **(B)** Genome browser snapshots showing two examples of L1 fusion genes derepressed in MORC2 mutant and CRISPRi treatments.

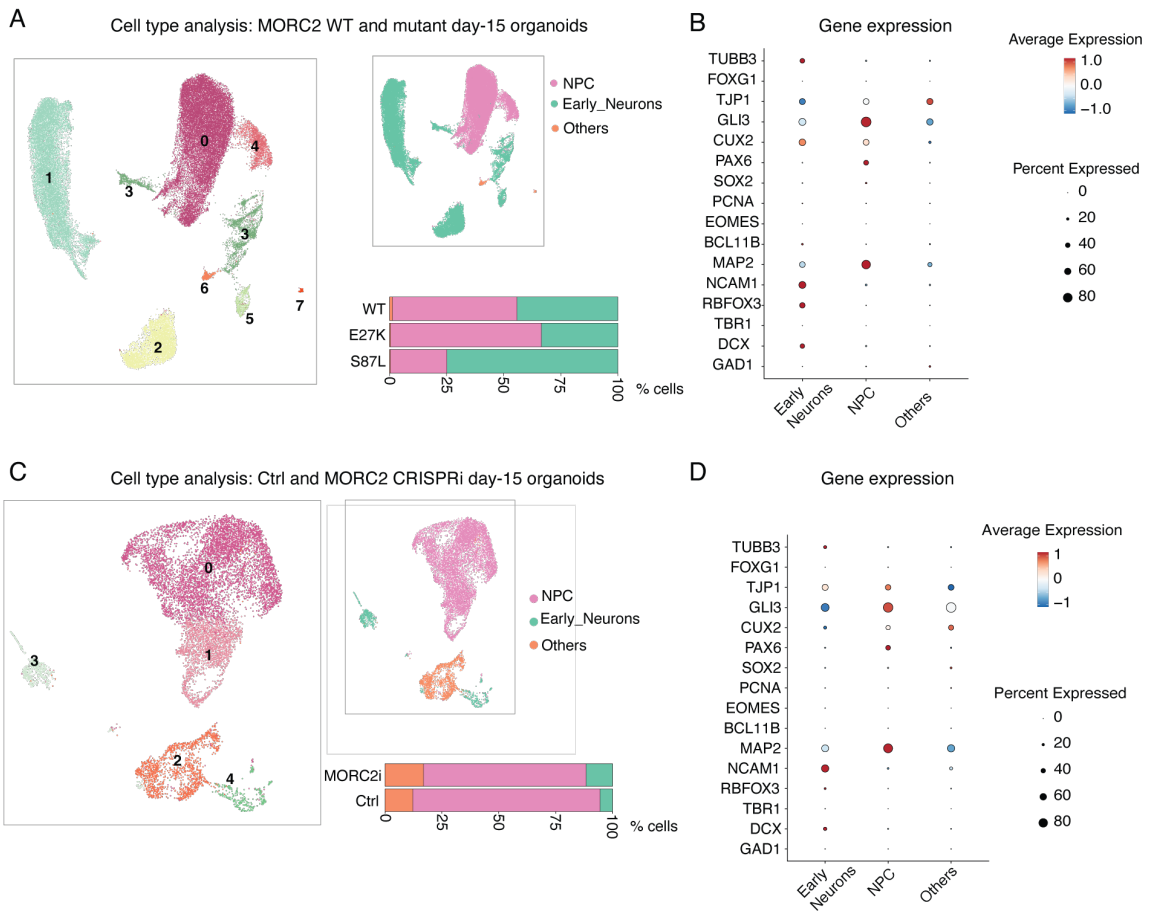

Supplementary Figure 5. Cell composition of day 15, unguided cerebral organoids. **(A)** Left/Middle: UMAP showing the cell types identified in MORC2-WT (4-5 organoids from n=4 batches/clones), MORC2-E27K (4-5 organoids from n=2 batches/clones) and MORC2-S87L mutant (4-5 organoids from n=2 batches/clones) unguided cerebral organoids. Bottom: bar plot showing percentage of the cell type composition of the MORC2 WT and MORC2-S87L mutant cerebral organoids. **(B)** Dot plot showing neuronal and NPC gene markers used to characterize the cell clusters. Dot size corresponds to the proportion of cells expressing the gene. Dot color indicates average expression in each cell type. **(C)** Left/Middle: UMAP showing the cell types identified in control (4-5 organoids from n=1 batch) and MORC2 CRISPRi (4-5 organoids from n=1 batch) unguided cerebral organoids. Bottom: bar plot showing percentage of the cell type composition of the control and MORC2 CRISPRi cerebral organoids. **(D)** Dot plot showing neuronal and NPC gene markers used to characterize the cell clusters. Dot size corresponds to the proportion of cells expressing the gene. Dot color indicates average expression in each cell type.

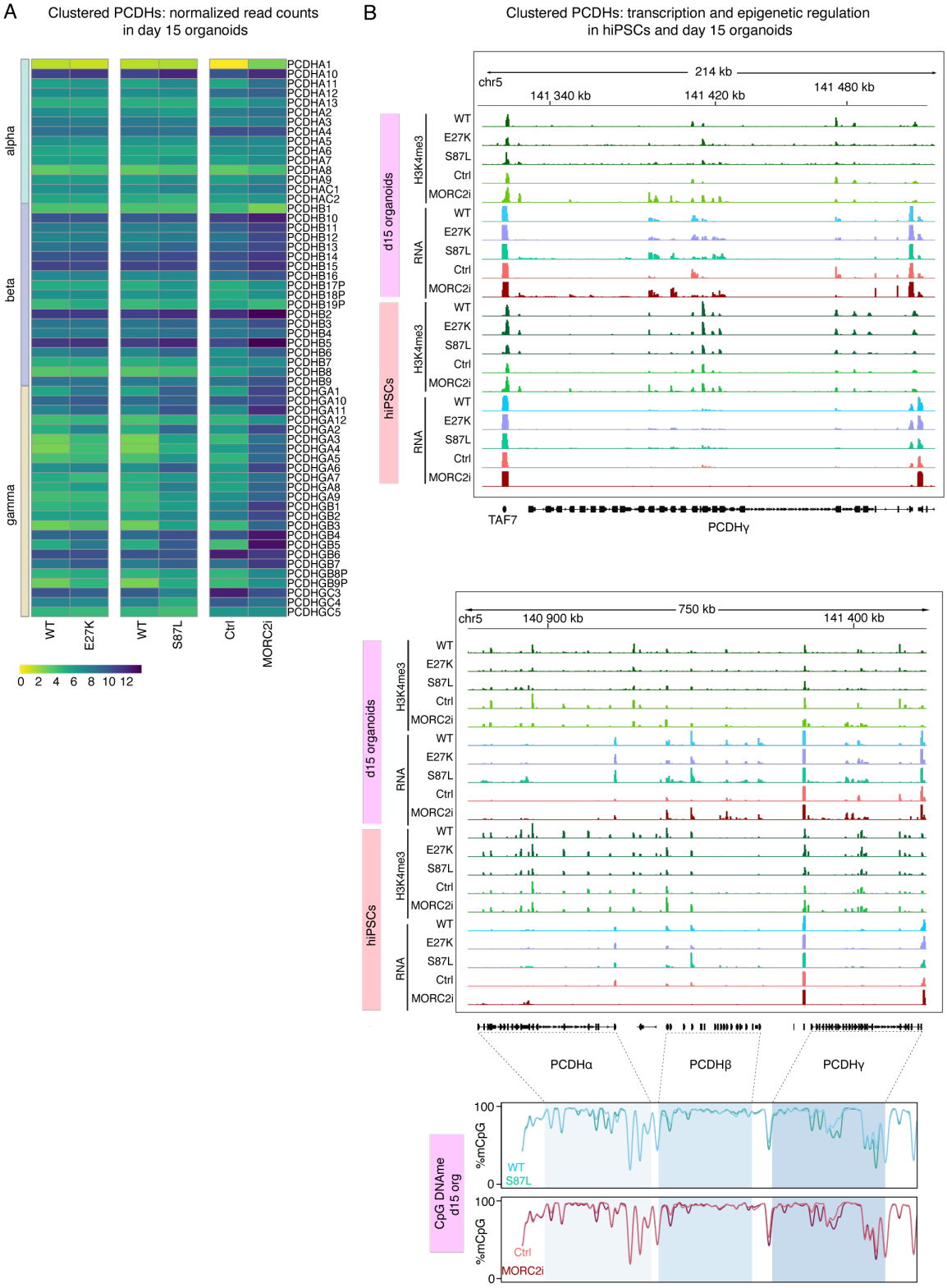

Supplementary Figure 6. (A) Unscaled heatmap showing normalized read counts of bulk RNA-seq data for clustered protocadherin genes (PCDHα, PCDHβ and PCDHγ) as calculated by DESeq2 in WT (n=9 samples from a total of 27 organoids differentiated from 3 iPSC lines across 3 batches,) E27K (n=9 samples from a total of 27 organoids differentiated from 2 iPSC lines across 2 batches) and S87L (n=9 samples from a total of 27 organoids differentiated from 2 iPSC lines across 2 batches) cell lines, and from Control (n=3 samples derived from 9 organoids differentiated from 1 bulk transduced cell line across 1 batch) and MORC2 CRISPRi (n=3 samples derived from 9 organoids differentiated from 1 bulk transduced cell line across 1 batch). **(B)** Genome browser

view of bulk RNA-seq and H3K4me3 CUT&RUN from organoid experiments of the PCDHγ cluster (top) and PCDHα, PCDHβ and PCDHγ clusters (center), and their mean percentage methylation profile (bottom). Data are representative of all replicates performed.

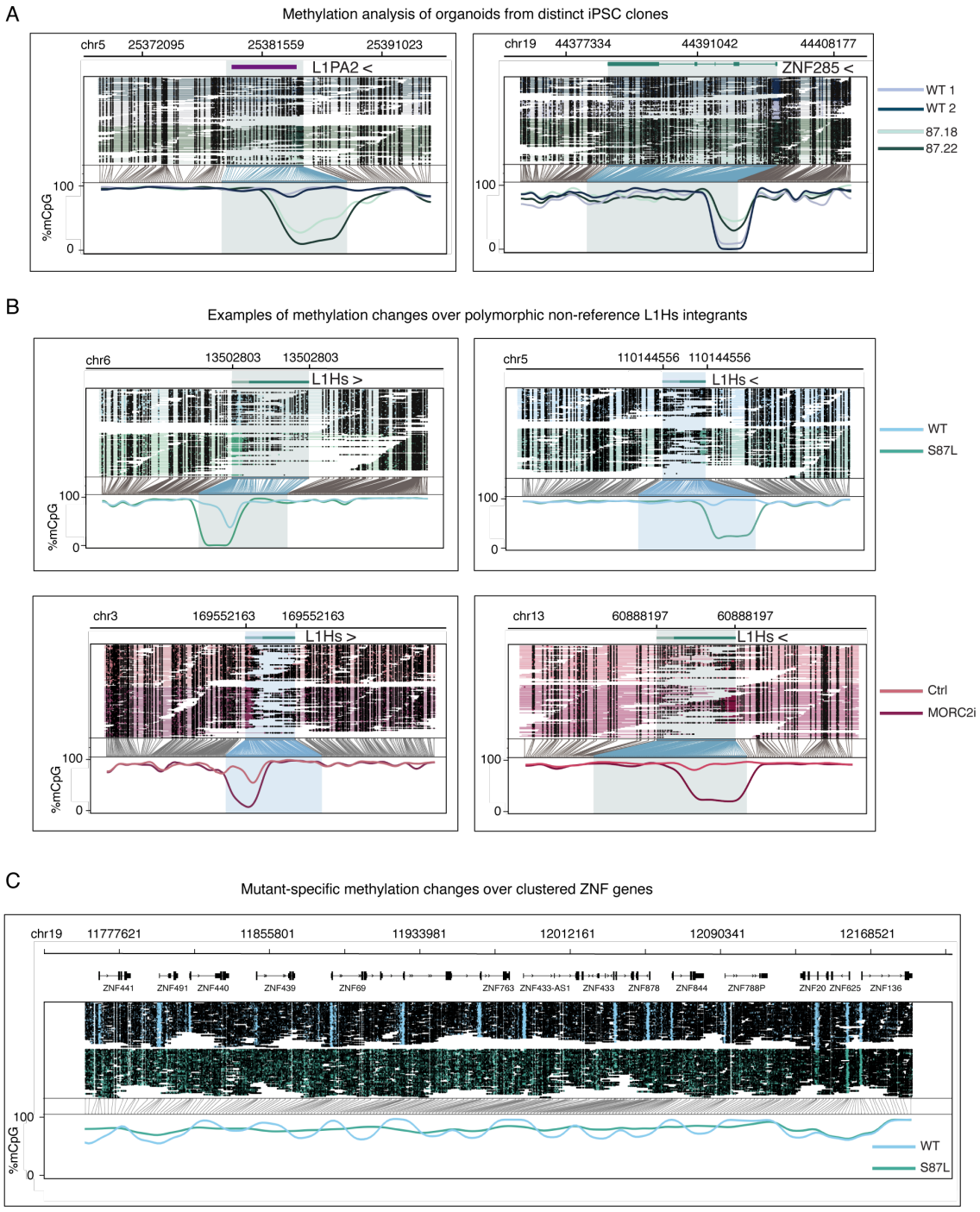

Supplementary Figure 7. (A) Aligned Nanopore reads showing CpG methylation across clones belonging to the WT (n=2) and S87L (n=2) cell lines over example L1 and ZNF gene loci. **(B)** Aligned Nanopore reads showing CpG methylation over examples of non-reference LINE1 insertions in WT and S87L cell lines, and Ctrl and MORC2 CRISPRi cell lines. **(C)** Aligned Nanopore reads showing long-range dysregulated CpG methylation over a ZNF gene cluster.